NAVAL POSTGRADUATE SCHOOL
Monterey, California

THESIS

AMBIENT NOISE DUE TO THE SHEARING OF THE BOUNDARY LAYER UNDER SEA ICE

by

Stephen J. Hipsey

December 1988

Co-Advisors

Robert S. Pritchard
Jeffrey A. Nystuen

Approved for public release; distribution is unlimited

REPORT DOCUMENTATION PAGE

1a Report Security Classification: Unclassified		1b Restrictive Markings	
2a Security Classification Authority		3 Distribution Availability of Report: Approved for public release; distribution is unlimited.	
2b Declassification Downgrading Schedule			
4 Performing Organization Report Number(s)		5 Monitoring Organization Report Number(s)	
6a Name of Performing Organization: Naval Postgraduate School	6b Office Symbol (*if applicable*): 35	7a Name of Monitoring Organization: Naval Postgraduate School	
6c Address (*city, state, and ZIP code*): Monterey, CA 93943-5000		7b Address (*city, state, and ZIP code*): Monterey, CA 93943-5000	
8a Name of Funding Sponsoring Organization	8b Office Symbol (*if applicable*)	9 Procurement Instrument Identification Number	
8c Address (*city, state, and ZIP code*)		10 Source of Funding Numbers	
		Program Element No	Project No / Task No / Work Unit Accession No

11 Title (*include security classification*): AMBIENT NOISE DUE TO THE SHEARING OF THE BOUNDARY LAYER UNDER SEA ICE (Unclassified)

12 Personal Author(s): Stephen J. Hipsey

13a Type of Report	13b Time Covered	14 Date of Report (*year, month, day*)	15 Page Count
Master's Thesis	From To	December 1988	93

16 Supplementary Notation

17 Cosati Codes			18 Subject Terms (*continue on reverse if necessary and identify by block number*)
Field	Group	Subgroup	Arctic ambient noise, Ambient noise under ice, Noise mechanisms

19 Abstract (*continue on reverse if necessary and identify by block number*)

The generation of ambient noise by physical processes dependent on shearing of the boundary layer under sea ice is investigated. Special attention is paid to the identification of individual noise-generating mechanisms and the assessment of their relative importance.

Recent studies of Arctic ambient noise are reviewed with specific reference to results showing particularly good or poor correlation between ambient noise levels and ice movement or relative current. Potential noise-generating mechanisms are described and categorized according to their small-scale driving forces and expected noise characteristics. More detailed quasi-objective investigations are then used to establish the relative importance of each mechanism as a contributor to the overall under-ice noise spectrum.

Flow/Mechanical mechanisms, involving ice sheet fracture as a result of wind and current-induced bending moments, are found to be unlikely contributors. Conversely, processes in which ice fragments in current-driven motion under the ice interact to cause bumping and grinding noises, appear to be of probable importance. Turbulent pressure fluctuations in the boundary layer under sea ice are shown to be of significance at low frequencies on a local scale. The role of resonant cavities in the under-surface of the ice does not appear, however, to be an important one.

20 Distribution Availability of Abstract	21 Abstract Security Classification	
☒ unclassified unlimited ☐ same as report ☐ DTIC users	Unclassified	
22a Name of Responsible Individual: A. Nystuen	22b Telephone (*include Area code*): (408) 646-2917	22c Office Symbol: 68Ny

DD FORM 1473,84 MAR

83 APR edition may be used until exhausted
All other editions are obsolete

Approved for public release; distribution is unlimited.

Ambient Noise Due to the Shearing of the Boundary Layer Under Sea Ice

by

Stephen J. Hipsey
Lieutenant, Royal Navy
B.Sc., Plymouth Polytechnic, 1981

Submitted in partial fulfillment of the
requirements for the degree of

MASTER OF SCIENCE IN PHYSICAL OCEANOGRAPHY

from the

NAVAL POSTGRADUATE SCHOOL
December 1988

ABSTRACT

The generation of ambient noise by physical processes dependent on shearing of the boundary layer under sea ice is investigated. Special attention is paid to the identification of individual noise-generating mechanisms and the assessment of their relative importance.

Recent studies of Arctic ambient noise are reviewed with specific reference to results showing particularly good or poor correlation between ambient noise levels and ice movement or relative current. Potential noise-generating mechanisms are described and categorized according to their small-scale driving forces and expected noise characteristics. More detailed quasi-objective investigations are then used to establish the relative importance of each mechanism as a contributor to the overall under-ice noise spectrum.

Flow Mechanical mechanisms, involving ice sheet fracture as a result of wind and current-induced bending moments, are found to be unlikely contributors. Conversely, processes in which ice fragments in current-driven motion under the ice interact to cause bumping and grinding noises, appear to be of probable importance. Turbulent pressure fluctuations in the boundary layer under sea ice are shown to be of significance at low frequencies on a local scale. The role of resonant cavities in the under-surface of the ice does not appear, however, to be an important one.

TABLE OF CONTENTS

LIST OF FIGURES

I. INTRODUCTION.

Recent strategic thinking has placed great emphasis on anti-submarine warfare in the ice-covered waters of the Arctic Ocean (Young, 1986). This emphasis is the chief driving force behind ever increasing efforts to fully comprehend and model underwater acoustics in this region. A significant proportion of this effort has been directed towards the study of ambient noise under the ice and in the marginal ice zone. The importance of being able to predict ambient noise stems from its variability and its influence on passive sonar performance.

The effectiveness of any form of passive sonar, be it shipborne, towed, air dropped or mounted on the sea bed, is described by the passive sonar equation. From Urick (1983)

$$SL - TL = NL - DI + DT$$

where

SL is the source level: a measure of the sound emitted by the target

TL is the transmission loss: the amount of attenuation experienced along the acoustic path from the target to the receiver

NL is the noise level: the level of background and self noise obscuring the signal at the receiver

DI is the directivity index: a measure of the directivity of the sonar equipment

DT is the detection threshold: the minimum signal level that can be detected by an operator using the sonar equipment.

It is the ability to accurately measure or predict the magnitude of the terms in this equation which permits the effective determination of passive sonar performance. A firm knowledge of the parameters which govern the passive sonar equation therefore allows an operator to plan both offensive and defensive operations with an invaluable degree of foresight. An example might be the ability to forecast a time period, or geographic location, offering poor passive sonar conditions in which a submarine might safely conduct noisy evolutions while avoiding detection by hostile forces. Conversely, a unit engaged in offensive operations against submarine targets under the ice would benefit from an ability to predict a good acoustic environment.

The magnitude of the source level term is dependent on the sound energy emitted by the object of the passive detection effort. It is therefore governed by engineering, naval architectural and tactical considerations not directly related to the environment. Transmission loss depends entirely on environmental factors, being a function largely of sea water and sea bed characteristics. Temperature and salinity gradients, both horizontal and vertical, are particularly important. Although this term is undoubtably important in fixing effective sonar ranges, variability over moderate distances and time periods is relatively small in Arctic waters. This means that good climatological, or better still, recently measured, profiles of temperature and salinity are usually adequate for sonar range prediction work over a broad area and for considerable time periods.

The noise level term is generally of the most crucial importance in the overall sonar performance prediction effort in Arctic waters. It depends to a large degree on the environment and is known to be highly variable both spatially and temporally. Noise level incorporates the effects of self noise, created by the hydrophone itself or by the platform on which it is mounted, and ambient noise from the surrounding water mass. Ambient noise from the environment is a variable factor depending on many environmental forcing functions. Its accurate prediction is crucial to the successful assessment of passive sonar performance.

The last two terms of the equation, directivity index and detection threshold, are functions of equipment design, operating technique and in the case of the latter, operator effectiveness.

Thus it can be seen that ambient noise prediction is an essential part of planning for Arctic operations. An additional utility can also be found in weapons, sensor, and underwater communications systems design, where a grasp of typical ambient noise levels is important.

Considerable effort has been directed towards the modelling and prediction of ambient noise under ice. The problem has been tackled in a variety of ways including empirical approaches, attempts to predict noise levels through the summation of emissions from sources and by consideration of energy budgets (Oard, 1987). Pritchard (1988) emphasised the need to investigate and understand the physics behind noise-generating processes on a local scale before modelling them and summing their effects at a particular location. The overall predicted noise would then be the sum of the noise intensities from many locations, generated by a variety of mechanisms and subject to transmission losses depending on receiver depth, source depth, range to the source and frequency. The resulting Arctic ambient noise model would be driven by outputs from existing

meteorological and ice dynamics models. A categorization scheme for noise-generating mechanisms was proposed, by Pritchard, based on forcing factors. Mechanisms important under compact ice conditions are separated into three areas

1. ridging effects which are driven by large scale ice stress and deformation
2. micro-cracking effects which are driven by local ice stress
3. effects dependent on the shearing of the boundary layer of the ocean under the ice.

It is the purpose of this study to identify and investigate any mechanisms which may fall into the last category. Such potential noise-generating mechanisms are catalogued as exhaustively as possible and categorized according to their small scale driving forces and expected noise characteristics. Investigations are then conducted with a view to establishing their importance, if any, in the overall generation of ambient noise under ice.

Many of the physical processes involved are highly complex, and some are poorly understood or the subject of current research. For this reason the investigations are to some degree subjective. An attempt has been made to model the physics in as elementary a fashion as possible and generally to draw inferences from 'order of magnitude' results.

Chapter II is a review of recent Arctic ambient noise research which considers the effects of boundary layer shear. The purpose of this brief review is twofold. Firstly to explore the fundamental concept that noise is caused by shearing of the boundary layer under ice, and secondly, to identify individual mechanisms which have been suggested as being responsible for noise. Evidence is sought to establish whether shearing in the oceanic boundary layer, in the form of ice movement through the water or water movement under stationary ice, is important as a forcing function for noise generation.

Chapter III outlines potential noise generating mechanisms and a proposed categorization scheme. The individual mechanisms are then investigated in Chapter IV with conclusions and a summary presented in Chapter V.

II. REVIEW OF CURRENT LITERATURE.

Previously published studies of under-ice ambient noise are fairly numerous and investigate a broad range of different forcing functions. Forcing by thermal effects were investigated by Ganton and Milne (1965) and Milne (1972) while forcing by pressure ridging and ice mechanics was studied by Pritchard (1984) and by Buck and Wilson (1986). Various other atmospheric forcing functions have also been studied by Payne (1964), Ganton and Milne (1965) and Greene and Buck (1978).

Three recent papers, Makris and Dyer (1986), Lewis and Denner (1988) and Waddell and Farmer (1988), consider shearing of the oceanic boundary layer in the form of ice movement or flow of water under ice as a forcing function. These papers are therefore reviewed briefly with the objective of highlighting results which tend to confirm or deny the importance of boundary layer shearing under ice as a forcing function for noise generation.

Makris and Dyer (1986) analysed low frequency ambient noise measurements and comprehensive environmental data from the 1982 FRAM IV expedition to the central Arctic ($83°N\ 20°E$). The octave band 10 - 20 Hz was taken as being representative of noise in the low frequency range and compared with temperature and various applied stress components. The underlying hypothesis was that:-

> Noise is created by ice fracture mechanisms proportional to the state of stress in the ice as induced by environmental loading.

Cross-correlation coefficients between the low frequency noise records and shear stresses due to the wind and current were found to be particularly high, 0.84, in both cases for 9.9-day records and 0.71 and 0.74, respectively, for 23.7-day records. The corresponding coefficient for tensile stress due to cooling was 0.15. Composite measurements, namely ice stress on the ice sheet's vertical section and the stress moment acting about the ice sheet's central horizontal plane, were also highly correlated with ambient noise, correlation coefficients being 0.81 and 0.87, respectively, for 9.9 day-records.

The general conclusion of the work was that low frequency pack ice noise correlates best with the moment due to opposing wind and current stresses acting on the ice and worst with air temperature.

Lewis and Denner (1988) studied the correlation between noise at 10, 32 and 1000 Hz and a number of parameters describing temperature and ice kinematics. The data analysed were obtained during the AIDJEX project in the Beaufort Sea during 1975-1976 and was exceptionally comprehensive. High quality positional data were available from some 40 satellite-tracked drifters which allowed the accurate determination of ice translational speed and differential kinematic parameters. Correlation coefficients were calculated for ambient noise levels at the above frequencies and the following parameters:

U, the translation rate of the ice

U^2, proportional to the kinetic energy of the ice

D, the divergence of the ice

$|D|$

V, the vorticity (rotation rate) of the ice

$|V|$

N, the normal deformation rate of the ice

S, the shear deformation rate of the ice

F, the temperature difference between the air and the ice

and

$(N^2 + S^2)^{1/2}$, the total deformation of the ice.

The results of these calculations are reproduced as Figure 1. The correlation obtained throughout between ambient noise and U, the simple translation rate of the ice measured by satellite tracking, is quite striking. In virtually all cases the correlation was the maximum observed for any of the parameters above. U correlated particularly well with 32 Hz noise in the summer (August 1975). This was attributed to the ice "rushing through the water". Another observation was that, in general, U correlated better than U^2, except at 1000 Hz. This suggests that pure ice motion is more important in producing noise than the kinetic energy of the floes, except at higher frequencies where collision events are probably more significant.

10 Hz	Correlations (percent variances)				
	Summer		Fall		Winter
	Station 10	Station 66	Station 10	Station 66	Station 10
U	...	...	0.72(52.5)	0.76(58.5)	0.60(35.9)
U^2	0.65(42.4)	0.70(48.9)	0.61(37.7)	0.74(55.4)	0.46(21.3)
D	0.48(23.2)	0.41(16.8)	0.07(0.5)	0.23(5.5)	−0.29(8.4)
V	0.47(22.5)	0.31(9.7)	−0.21(4.4)	−0.48(22.7)	0.05(0.2)
N	−0.04(0.2)	−0.11(1.2)	−0.06(0.4)	0.1(0.0)	0.01(0.0)
S	0.09(0.9)	−0.02(0.0)	−0.46(21.0)	−0.40(16.2)	−0.10(1.1)
F	0.02(0.0)	0.06(0.4)	0.06(0.4)	0.10(1.0)	0.18(3.0)
$\|D\|$	0.40(15.9)	0.50(25.1)	0.41(17.0)	0.58(33.4)	0.49(24.0)
$\|V\|$	0.39(15.2)	0.31(9.5)	0.46(20.9)	0.67(44.6)	0.50(25.4)
$(N^2+S^2)^{1/2}$	0.23(5.3)	0.38(14.3)	0.63(39.4)	0.72(51.9)	0.39(15.4)
Maximum correlation	0.73	0.74	0.79	0.86	0.76
32 Hz					
	Summer		Fall		Winter
	Station 10	Station 66	Station 10	Station 66	Station 10
U	0.74(54.6)	0.82(67.3)	0.70(49.2)	0.70(48.7)	0.66(43.7)
U^2	0.72(52.3)	0.80(63.6)	0.59(35.4)	0.62(38.8)	0.56(31.1)
D	0.28(8.1)	0.40(15.7)	0.09(0.8)	0.18(3.2)	−0.38(14.2)
V	0.41(16.5)	0.37(13.6)	−0.21(4.3)	−0.42(17.6)	0.12(1.4)
N	0.01(1.2)	0.0(0.0)	−0.09(0.8)	−0.20(0.1)	−0.04(0.2)
S	0.06(0.3)	0.09(0.8)	−0.49(24.2)	−0.34(11.8)	−0.23(5.3)
F	0.03(0.1)	0.05(0.2)	0.01(0.0)	0.07(0.4)	0.13(1.5)
$\|D\|$	0.27(7.2)	0.40(16.3)	0.35(12.4)	0.55(29.9)	0.42(18.0)
$\|V\|$	0.33(10.8)	0.35(12.5)	0.44(19.0)	0.59(34.4)	0.49(23.9)
$(N^2+S^2)^{1/2}$	0.30(8.7)	0.42(17.4)	0.57(32.3)	0.65(41.8)	0.38(14.5)
Maximum correlation	0.76	0.84	0.76	0.78	0.78
1000 Hz					
	Summer		Fall		Winter
	Station 10	Station 66	Station 10	Station 66	Station 10
U	0.63(40.3)	...	0.34(11.5)	0.28(7.7)	0.60(35.5)
U^2	0.65(41.7)	0.76(58.1)	0.28(7.6)	0.20(4.0)	0.62(38.8)
D	0.30(8.7)	0.23(5.3)	0.11(1.3)	0.26(6.6)	−0.27(7.5)
V	0.44(19.0)	0.27(7.1)	−0.08(0.6)	−0.20(3.9)	0.01(0.0)
N	−0.09(0.8)	0.0(0.0)	−0.11(1.3)	0.01(0.0)	−0.11(1.3)
S	0.08(0.6)	−0.07(0.5)	−0.32(10.1)	−0.06(0.4)	−0.31(9.4)
F	0.0(0.0)	0.07(0.5)	−0.08(0.6)	0.04(0.2)	−0.07(0.1)
$\|D\|$	0.20(3.9)	0.19(3.8)	0.17(2.9)	0.40(16.3)	0.30(8.8)
$\|V\|$	0.23(5.5)	0.13(1.7)	0.16(3.4)	0.28(7.9)	0.38(14.1)
$(N^2+S^2)^{1/2}$	0.14(1.9)	0.32(10.1)	0.11(1.3)	0.24(5.7)	0.36(12.8)
Maximum correlation	0.69	0.81	0.49	0.45	0.67

Figure 1. Linear correlation coefficients between ambient noise and ice kinematic parameters (from Lewis and Denner, 1988).

Overall this work seems to emphasize the importance of ice movement in the generation of ambient noise. Although no particular mechanisms are mentioned, the role of shearing in the oceanic boundary layer appears to be of probable significance.

Waddell and Farmer (1988) describe the noise resulting from the break-up of land fast ice in Amundsen Gulf in the Canadian Archipelago. Although the study was in fact motivated by the possibility that ice conditions could be monitored acoustically, the conclusions are of some interest here.

Data collected over a 127-day period from April to August 1986 included ambient noise over the frequency range 300 Hz to 14.5 kHz, current measurements and meteorological observations. Currents in the area are strongly influenced by the tides. This is shown in Figure 2 which also depicts time series of longwave infra-red, ambient noise and air temperature for a 10-day period in June.

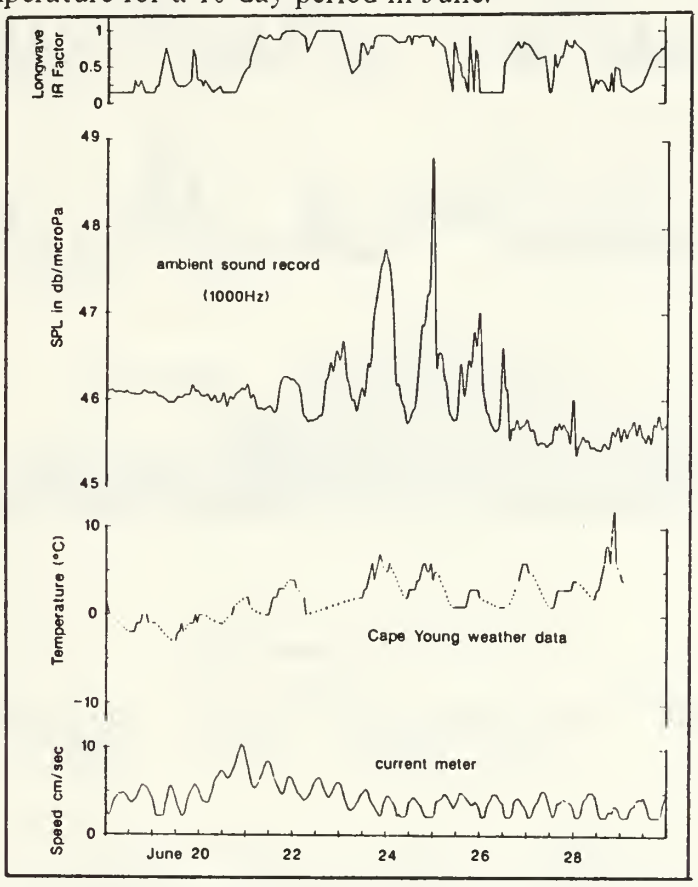

Figure 2. Time series of ambient noise and various environmental parameters (Waddell and Farmer, 1988).

Initially, when the ice was consolidated and land fast, there was no obvious correlation between the current meter observations and ambient noise. A more marked correspondence was noted between noise and atmospheric factors. A strong northerly current, developing in July, however, coincided with a sharp increase in noise levels as the ice near the recording instruments began to break up (see Figure 3).

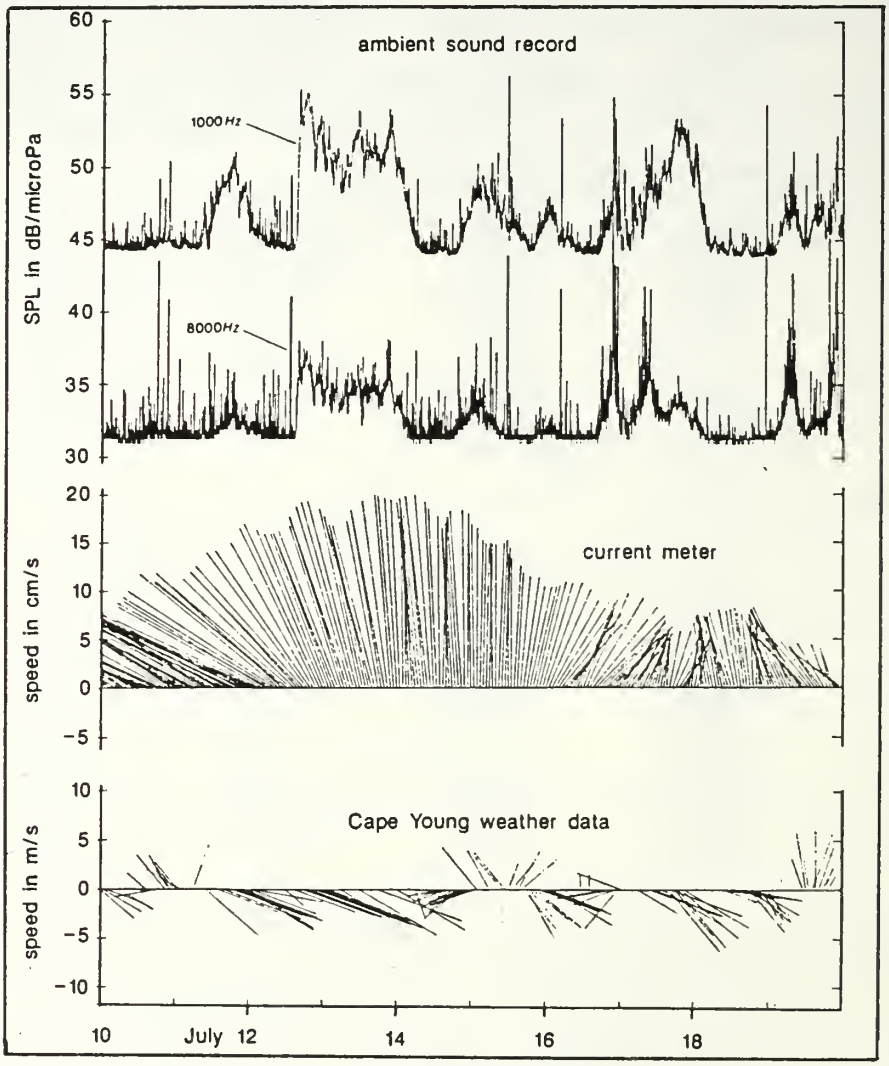

Figure 3. Time series showing the increase in ambient noise levels with increased current and ice breakup (Waddell and Farmer, 1988).

These results seem to indicate that when ice is landfast and static, a moderate current under it does not create discernable noise in the range 300Hz to 14.5 kHz. When the ice cover is in motion, however, significant correlations can be found between current speeds and high frequency noise. This is probably be due to collisions and cracking during ice breakup.

As a general summary, the studies done by Makris and Dyer (1986) support the idea that low frequency (10-20 Hz) noise results from opposing wind and current stresses acting on the ice. The results of Lewis and Denner (1988) show strong correlation between noise and ice translational speed which is proportional to the relative current under the ice. Waddell and Farmer showed that little noise results from relative current under stationary ice.

III. POTENTIAL NOISE GENERATING MECHANISMS.

Ambient noise due to shearing of the boundary layer under sea ice could be caused by a number of different mechanisms. Little or nothing has been written about the detailed processes involved and in some cases the physical processes are sufficiently complex to prohibit meaningful analytical investigation.

A number of potential noise-generating mechanisms are put forward here. The list is not intended to be exhaustive but most mechanisms which appear to have any possibility of being relevant to real world conditions are included. Some mechanisms appear intuitively more important than others while some may seem a little obscure. All are are included in this chapter and will be investigated to a greater or lesser degree in Chapter IV.

A. A CATEGORIZATION SCHEME.

Two broad categories of potential noise generating mechanisms have been identified. Firstly, *Flow/Mechanical* mechanisms which involve mechanical interaction between the sea and the ice cover and produce sound through cracking or impactive events. Secondly, *Flow* mechanisms which are purely a function of fluid flow in the presence of the solid ice boundary.

The potential mechanisms are therefore divided and ordered in this study according to these criteria. Figure 4 summarizes the mechanisms that have been considered and their relative positions in this scheme of organisation. Figure 5 is a schematic summary showing the partition of Flow/Mechanical and Flow mechanisms.

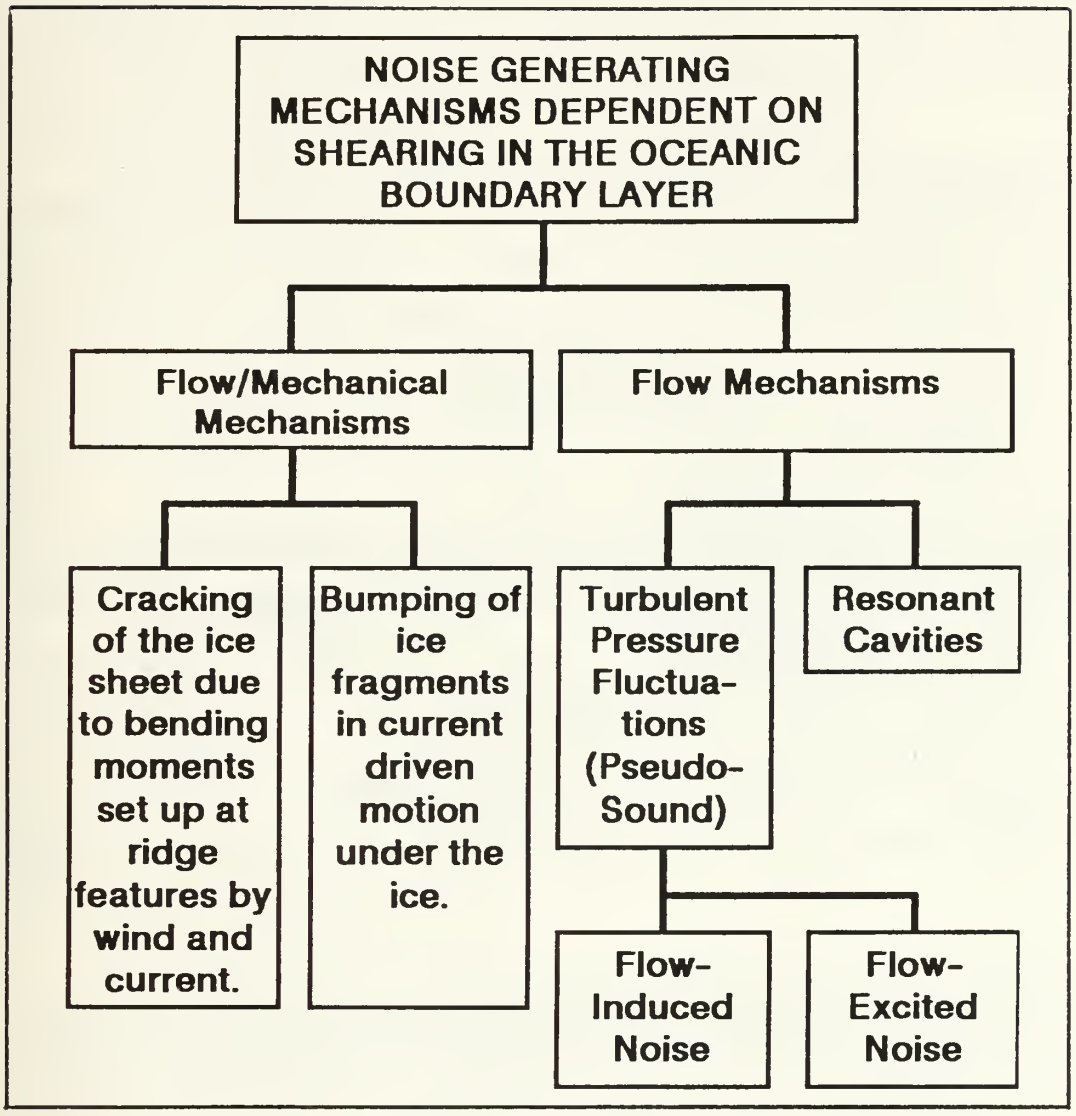

Figure 4. An overview of potential noise-producing mechanisms.

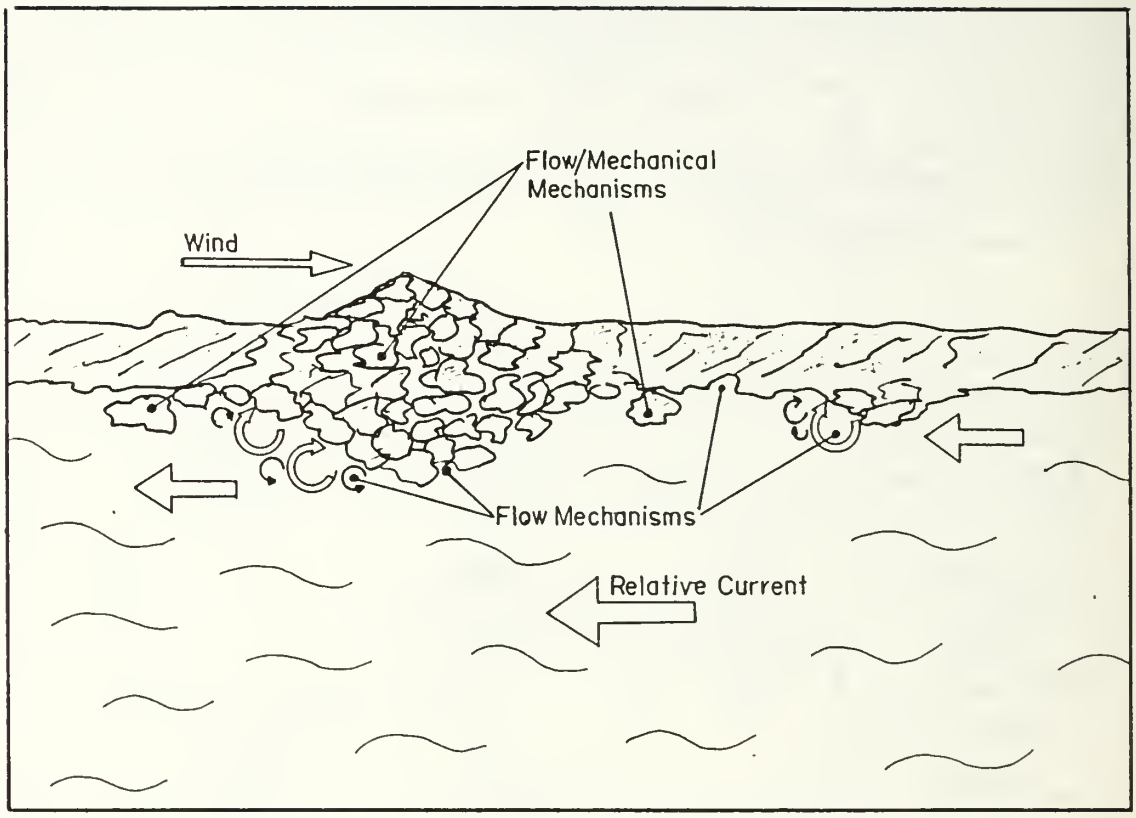

Figure 5. A schematic summary showing the partition of Flow/Mechanical and Flow mechanisms.

B. FLOW/MECHANICAL MECHANISMS.

1. Cracking Noise Due to Wind/Current-Induced Moments.

The concept of opposing wind and current stresses inducing moments in the Arctic ice cover was originated by Makris and Dyer (1986). Although no detailed description of the mechanism itself was presented, the high correlation obtained in the FRAM IV data, between noise and the stress moment acting about the ice sheet's horizontal plane, indicates the potential importance of this mechanism.

In an attempt to investigate the detailed mechanics of the processes involved, the wind and current stresses are taken to have most effect on features with some vertical extent. Pressure ridges or ice hummocks present obvious points where winds and currents could act to set up bending moments in the ice sheet which might possibly lead to ice fracture and therefore noise. The magnitudes of such bending moments are a function not only of the relative velocities of the wind and under-ice current, but also of the size and shape of the ridge and of the thickness and general nature of the ice sheet itself.

Maximum opposing wind and current velocities are most likely to occur when the ice is in a low-stress state with some degree of wind driven motion. Ice in a static state is less likely to be subjected to strong induced moments as the geostrophic and tidal currents in the open Arctic tend to be relatively weak. Wind and current stresses will also be greater in areas of highly deformed ice cover as drag there is more pronounced. Fracture as a result of induced bending moments may not neccessarily be more likely, however, as significant deformation is often coincident with greater ice thickness, lower salinity and therefore greater strength.

2. Ice Fragment Bumping.

The importance of ice collisions in the production of ambient noise has been recognized in several works (Diachok and Winokur ,1974; Shepard, 1979) and is an established mechanism when considered on a large scale, i.e., floe-floe interactions. The presence and movement of significant amounts of ice debris under sheet ice is also documented (Zubov, 1943; Buck and Wilson, 1986). A potential noise generation process therefore exists in any pack ice covered region where deformation events create quantities of loose fragmented material which can be moved around by a relative current. Noise from this source is likely to be aurally detectable and characterized by *bumping* or *grinding* sounds.

C. FLOW MECHANISMS.

1. Noise From Turbulence.

Turbulence is a recognized source of low frequency noise in the open ocean (Wenz, 1962; 1972). Although the processes by which it is radiated are exremely inefficient and its far field effects are minimal, the direct effect on hydrophones within turbulent flows can be significant. This is because the pressure fluctuations impinge directly on the active surfaces of hydrophones which react by generating an electrical signal. Thus turbulent pressure fluctuations can cause a type of self-noise whose effects may be significant at very low frequencies.

In the Arctic the situation is complicated by the presence of ice cover. The ice acts as a boundary of variable roughness past which water flows. In addition, the ice sheet itself may play a role in the radiation of turbulence noise to ranges beyond the actual source region. Turbulent self-noise has been recognised as a possible contaminant of Arctic ambient noise data by Makris and Dyer (1986) and is included as a noise-generating mechanism in its own right.

Flow-induced noise and flow-excited noise are described briefly in Chapter IV as potential mechanisms by which the effects of turbulent pressure fluctuations are radiated to the far field.

2. Resonant Cavities.

The under-surface of floating ice in Arctic regions is, by its very nature, rough, deformed and pitted with cavities caused by melting, fracture or brine rejection. Such holes or cavities present a potential noise source when water is in motion across their openings. Flow may be the result of ice motion or currents under static ice and could excite resonant responses in these cavities.

No known reference has been made to the possibility that resonant cavities might be responsible for under-ice noise but similar above-water features are certainly capable of producing noise in strong winds. Noise from hull cavity resonance is also well known in naval architecture (Blake, 1986).

The parameters affecting the frequency and intensity of sound from resonant cavities would be cavity size, shape and water flow speed.

IV. AN INVESTIGATION OF POTENTIAL NOISE MECHANISMS.

A. FLOW/MECHANICAL MECHANISMS.

1. Wind/Current-Induced Moments at Pressure Ridges.

The action of a current relative to an ice field on submerged pressure ridge keels and the action of the wind on their above water sails gives rise to a potential flow mechanical noise-generation mechanism. The moment set up by these forces may be enough to cause cracking and cracking noise in the ice sheet close to the ridge features.

The moment M_k due to water pressure on the ridge keels is likely to be reinforced by wind action on corresponding sail formations causing a moment M_s (see Figure 6). This is particularly so when internal stresses within the local ice field are low and motion is largely due to wind-induced free drift. The applied moment M_a is therefore a function of the wind velocity V_w, the relative current velocity V_c and the pressure ridge geometry. M_a is the sum of M_k the moment caused by the relative current on the keel and M_s the moment on the sail due to the wind.

This functional relationship is investigated below by assuming an idealized pressure ridge model after Wright et al. (1978) and Paquette and Bourke (1988). The geometry of this model is illustrated in Figure 7.

It is assumed that

1. the system is in local isostatic equilibrium when $V_w = V_c = 0$
2. the ridge is symmetrical about point O as shown in Figure 7, with dimensions governed by local isostatic balance
3. the density of the ice is homogeneous throughout with an equal percentage of void in the sail and keel structures
4. the surface of the ice sheet, sail and keel are perfectly smooth
5. the wind velocity $v_w(z)$ and relative current velocity $v_c(z)$ vary linearly with height and depth as shown in Figure 8.

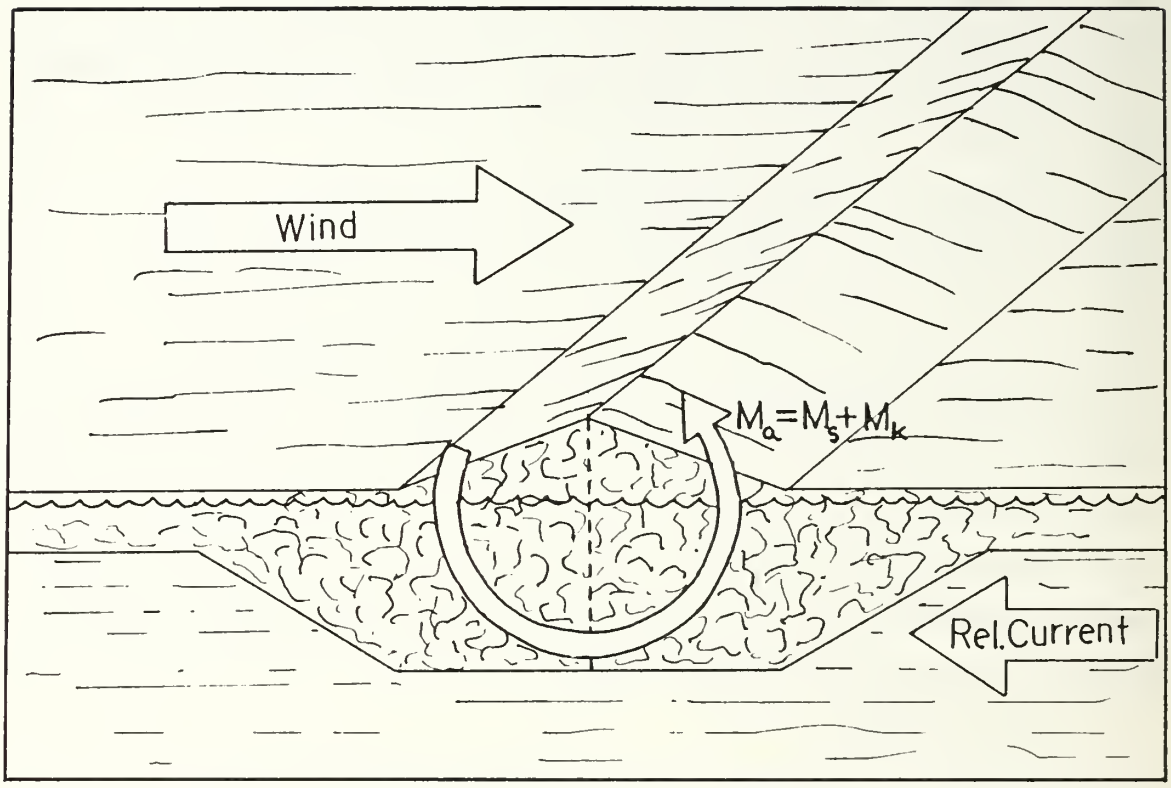

Figure 6. The action of the wind and relative current on a pressure ridge feature.

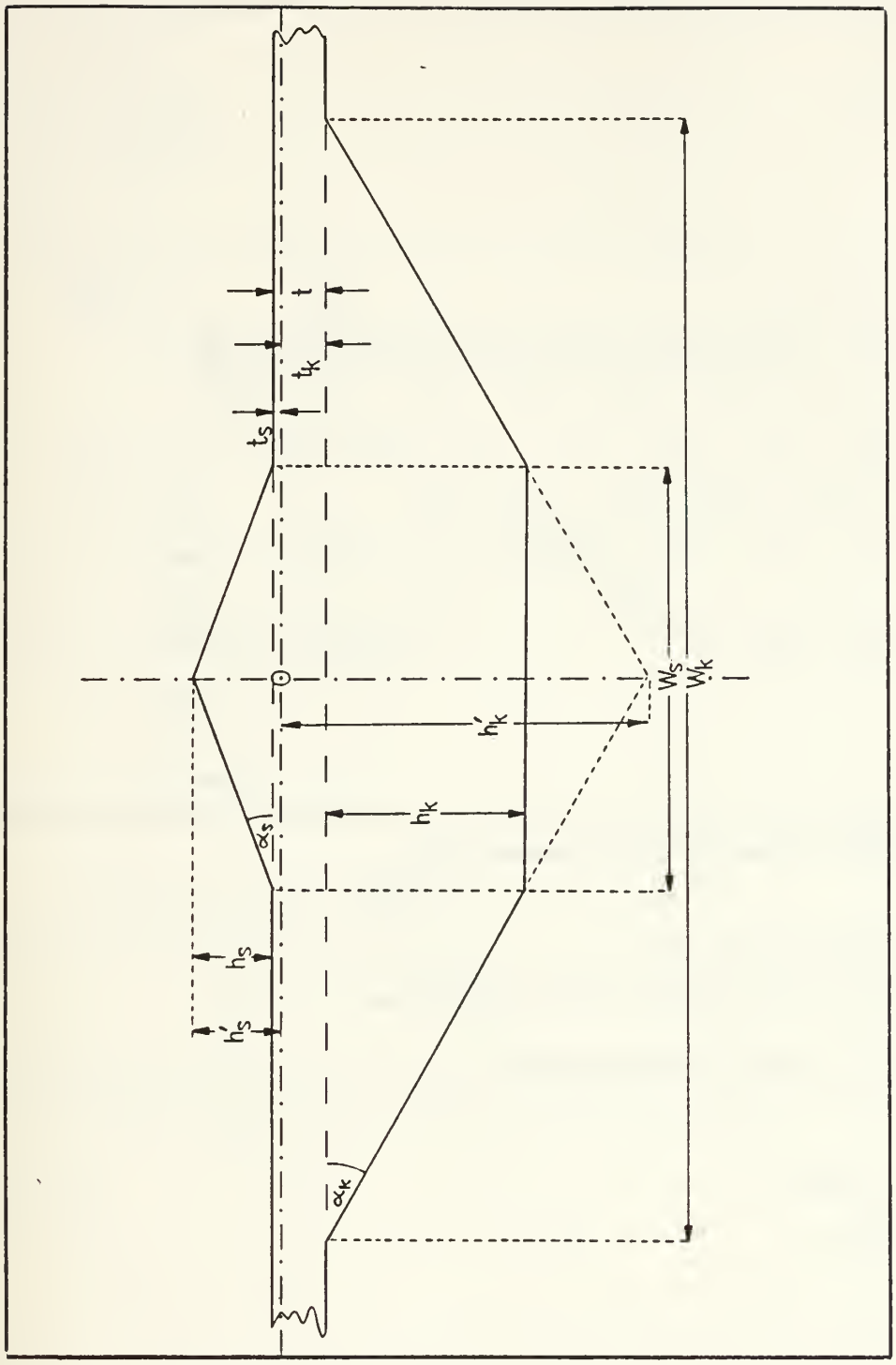

Figure 7. The idealized pressure ridge model.

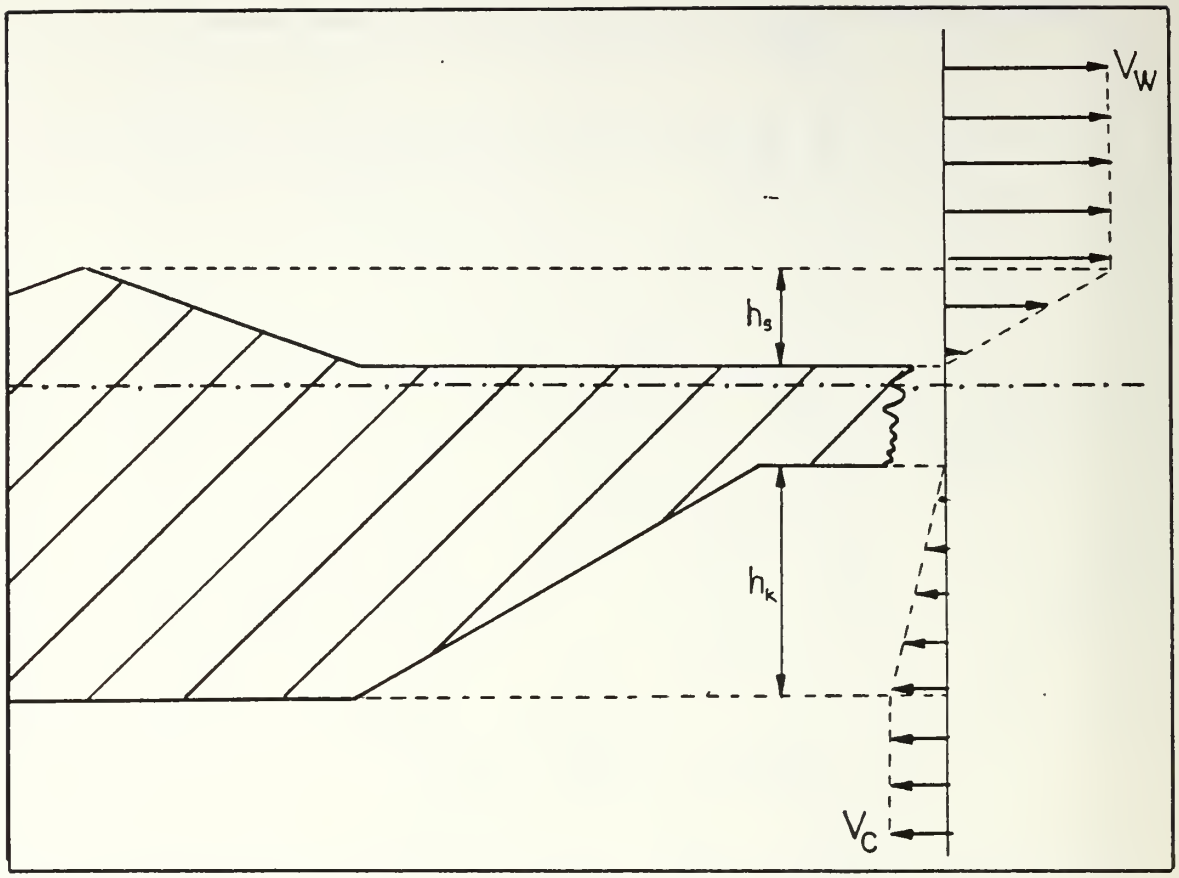

Figure 8. The assumed linear wind/current profile.

a. Ridge Model Geometry.

From the assumption of isostatic equilibrium

$$\tfrac{1}{2} h_s W_s \rho_i = (h_k W_s + \tfrac{1}{2} h_k (W_k - W_s))(\rho_w - \rho_i) \qquad (1)$$

where

ρ_w is the water density

ρ_i is the ice density

From Figure 7

$$W_k - W_s = \frac{2h_k}{\tan \alpha_k} \tag{2}$$

and

$$W_s = \frac{2h_s}{\tan \alpha_s} \tag{3}$$

so

$$W_k = \frac{2h_k}{\tan \alpha_k} + W_s \tag{4}$$

Substituting (2) and (3) into (1) and rearranging

$$\frac{h_s^2}{h_k^2}\left(\frac{\rho_i}{\rho_w - \rho_i}\right) - 2\frac{h_s}{h_k} - \frac{\tan \alpha_s}{\tan \alpha_k} = 0$$

Solving this quadratic in $\left(\frac{h_s}{h_k}\right)$

$$\frac{h_s}{h_k} = \frac{1 + \left(1 + \left(\frac{\rho_i}{\rho_w - \rho_i}\right)\frac{\tan \alpha_s}{\tan \alpha_k}\right)^{1/2}}{\left(\frac{\rho_i}{\rho_w - \rho_i}\right)} \tag{5}$$

Now taking typical values for ρ_i and ρ_w as 920 kg m^{-3} and 1026 kg m^{-3}, respectively, and $\alpha_k = 30°$, $\alpha_s = 20°$ (from Wright et al., 1978)

$$\frac{h_s}{h_k} \simeq 0.41 \tag{6}$$

also from Figure 7

$$h_k' = t_k + h_k + \frac{W_s}{2} \tan \alpha_k$$

or

$$h_k' = h_k + h_s \frac{\tan \alpha_k}{\tan \alpha_s} + t_k \tag{7}$$

Since the ice sheet itself can also be assumed isostatically balanced

$$t_s \rho_i = t_k(\rho_w - \rho_i) \tag{8}$$

and since

$$t = t_s + t_k$$

$$t_k = t \frac{\rho_i}{\rho_w} \simeq 0.9t \tag{9}$$

and

$$t_s = t \frac{(\rho_w - \rho_i)}{\rho_w} \simeq 0.1t \tag{10}$$

Substituting (9) into (7)

$$h_k' = h_k + h_s \frac{\tan \alpha_k}{\tan \alpha_s} + t \frac{\rho_i}{\rho_w}$$

Further substituting numerical values for α_s, α_k and h_k from (6)

$$h_k' \simeq 4h_s + t_k \tag{11}$$

or

$$h_k' \simeq 1.7h_k + t_k \tag{12}$$

From the geometry of the sail

$$h_s' = h_s + t_s \tag{13}$$

and from (10)

$$h_s' = h_s + t\frac{(\rho_w - \rho_i)}{\rho_w}$$

so

$$h_s' \simeq h_s + 0.1t \tag{14}$$

Now that functional relationships have been established between the various ridge dimensions, an equation for M_s, the moment caused by wind action on the sail about point O can be found (see Figure 9).

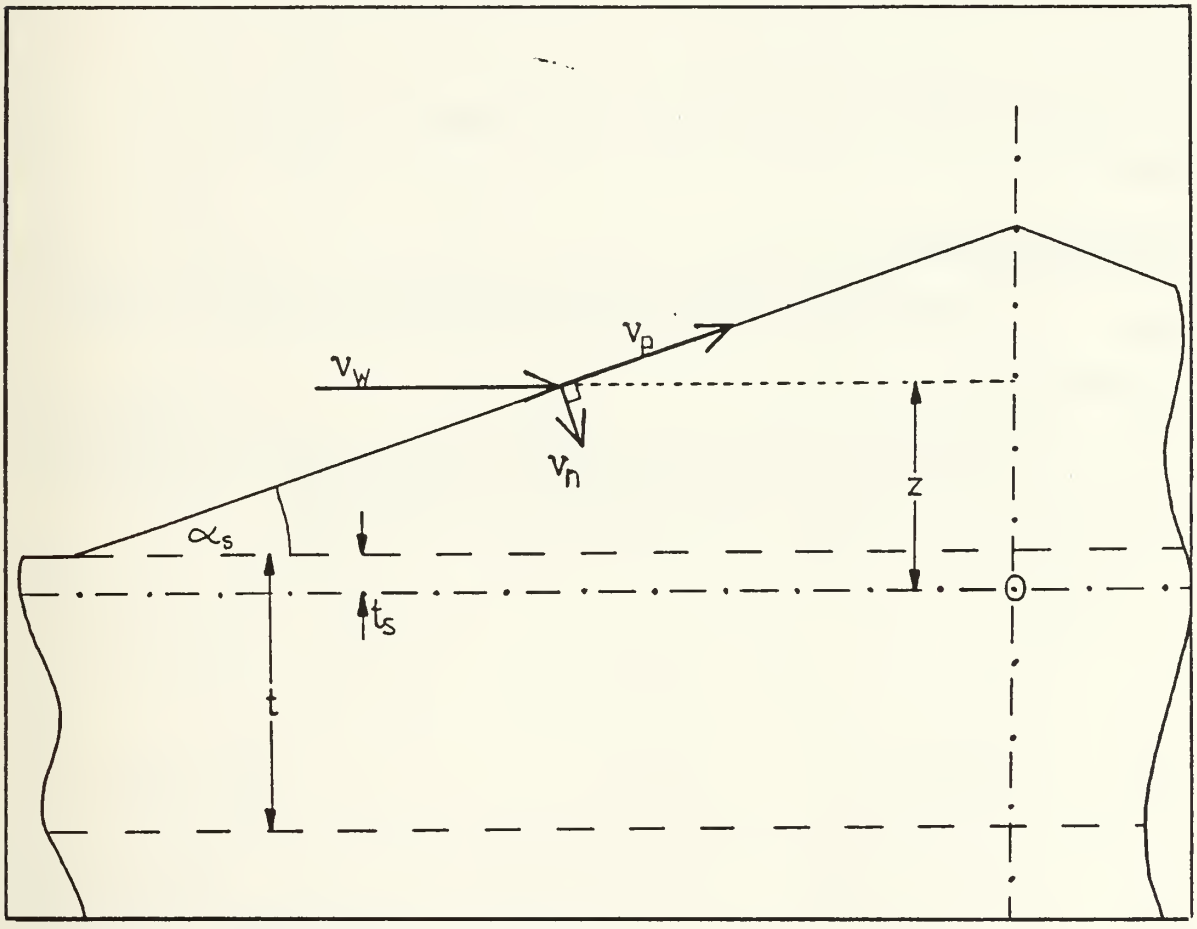

Figure 9. Wind action on the ridge sail.

b. The Moment Caused by Wind Action on the Sail.

Using concepts from Zubov (1943) and the theory for a fluid jet acting on a flat plate (Hannah & Hillier, 1970) the wind velocity v_w at height z above sea level can be resolved into two components: v_p the component parallel to the surface of the ridge sail and v_n normal to this surface.

$$v_p = v_w \cos \alpha_s \tag{15}$$

$$v_n = v_w \sin \alpha_s \tag{16}$$

At the windward surface of the sail v_n causes a dynamic force. v_p has no effect if the surface of the sail is perfectly smooth. The resulting force P is equal to the loss of momentum to the sail per second. So

$$P = \dot{m} v_w \sin \alpha_s \quad \text{kg m s}^{-2}$$

where

$\dot{m}$ is the mass of fluid (air) incident on the sail at height z, per second.

Then

$$P = \rho_a v_w^2 \sin \alpha_s \quad \text{kg m s}^{-2} \tag{17}$$

where

ρ_a is the air density.

The moment $m_s(z)$ about point O is given by the product of the length of the lever arm ℓ and the component P_ℓ, of P, normal to ℓ (see Figure 10).

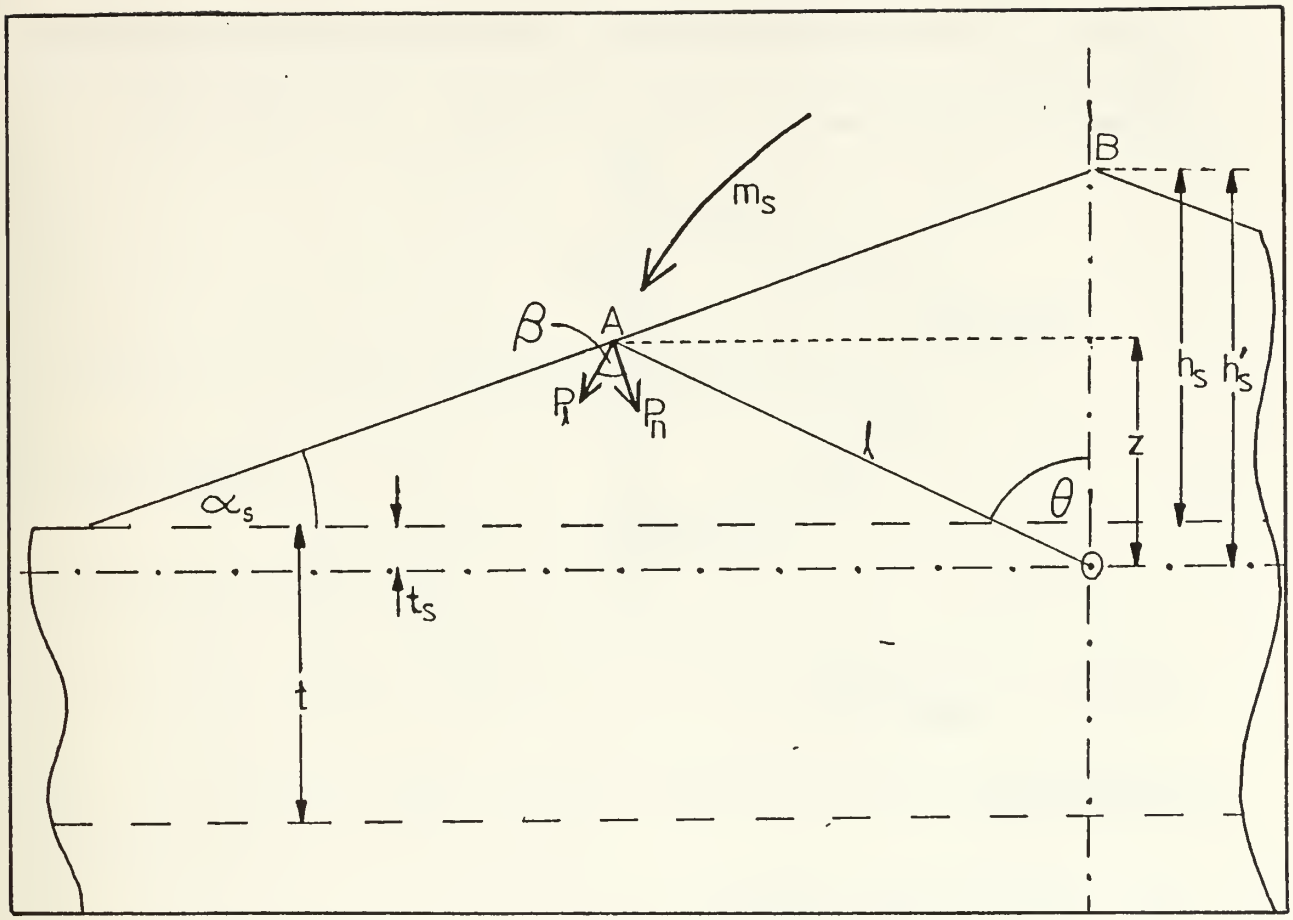

Figure 10. Moment about O, the point of symmetry, due to the wind.

From Figure 10

$$P_\ell = P_n \cos \beta$$

and

$$\beta = \pi/2 - \theta + \alpha_s$$

so

$$P_\ell = P \sin(\theta - \alpha_s)$$

and from (17)

$$P_\ell = \rho_a v_w^2 \sin \alpha_s \sin(\theta - \alpha_s) \qquad (18)$$

Now $\sin(\theta - \alpha_s)$ can be found in terms of h_s', ℓ, α_s and z by considering triangle OAB, (see Figure 11).

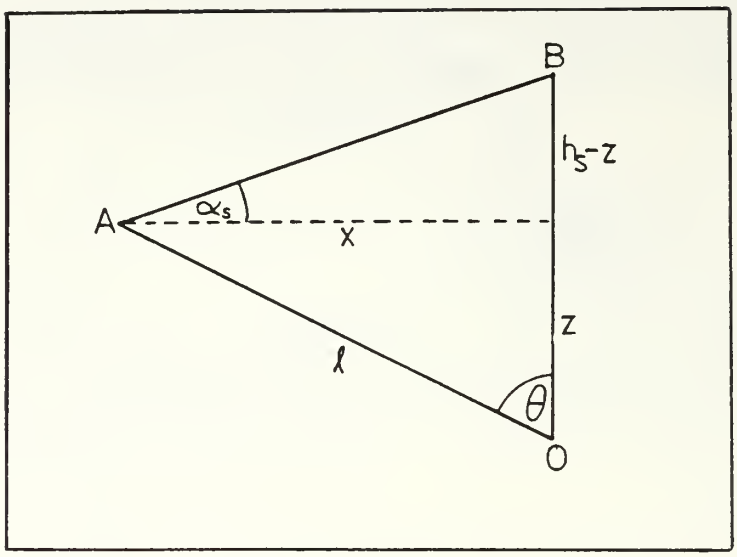

Figure 11. Triangle OAB.

From Figure 11

$$\sin(\theta - \alpha_s) = \sin\theta \cos\alpha_s - \cos\theta \sin\alpha_s$$

or

$$\sin(\theta - \alpha_s) = \frac{x \cos\alpha_s - z \sin\alpha_s}{\ell}$$

where

$$x = \frac{h_s' - z}{\tan\alpha_s}$$

so

$$\sin(\theta - \alpha_s) = \frac{h_s' \cos^2\alpha_s - z}{\ell \sin\alpha_s} \tag{19}$$

Substituting (19) into (18)

$$P_\ell = \frac{\rho_a v_w^2 (h_s' \cos^2\alpha_s - z)}{\ell} \tag{20}$$

and

$$m_s(z) = \ell P_\ell = \rho_a v_w^2 (h_s' \cos^2\alpha_s - z) \tag{21}$$

If the wind shear is linear, as outlined in the assumptions above

$$v_w(z) = \frac{V_w(z - t_s)}{h_s} \tag{22}$$

so substituting (22) into (21)

$$m_s(z) = \frac{\rho_a V_w^2}{h_s^2} (z - t_s)^2 (h_s' \cos^2\alpha_s - z) \tag{23}$$

The total moment M_s on the sail about point can now be found by integrating with respect to z between t_s and h_s'

$$M_s = \frac{\rho_a V_w^2}{h_s^2} \int_{t_s}^{h_s'} (z - t_s)^2 (h_s' \cos^2\alpha_s - z) dz \tag{24}$$

or

$$M_s = \frac{\rho_a V_w^2}{12 h_s^2} (h_s'^4 (4\cos^2\alpha_s - 3) + h_s'^3 t_s (8 - 12\cos^2\alpha_s) + h_s'^2 t_s^2 (6 - 12\cos^2\alpha_s) - 4h_s' t_s^3 \cos^2\alpha_s + t_s^4)$$

From (13)

$h_s' = h_s + t_s$

so

$$M_s = \frac{\rho_a V_w^2}{12} (h_s^2(4\cos^2\alpha_s - 3) + h_s t_s(4\cos^2\alpha_s - 4))$$

or

$$M_s = \rho_a V_w^2 h_s^2 C_s \tag{25}$$

where C_s is a form coefficient dependent on the geometry of the ridge.

$$C_s = \frac{1}{12}\left(4\cos^2\alpha_s - 3 + \frac{t_s}{h_s}(4\cos^2\alpha_s - 4)\right) \tag{26}$$

If $\alpha_s \simeq 20°$ and $t_s \simeq 0.1t$

$$C_s \simeq \left(44 - 4\frac{t}{h_s}\right) \times 10^{-3} \tag{27}$$

Figure 12 shows C_s plotted against h_s for various values of t. Note that $C_s \simeq 0.04$ for sail heights greater than one metre and is virtually independent of t. If α_s, the slope of the sail, is allowed to vary, an interesting effect is noticeable (see Figure 13). Where $\alpha_s \gtrsim 28°$, C_s reverses sign, i.e., the result is a moment in the opposite direction. This could be relevant when considering young, relatively unweathered ridge features where slopes may be greater than the 20° assumed above.

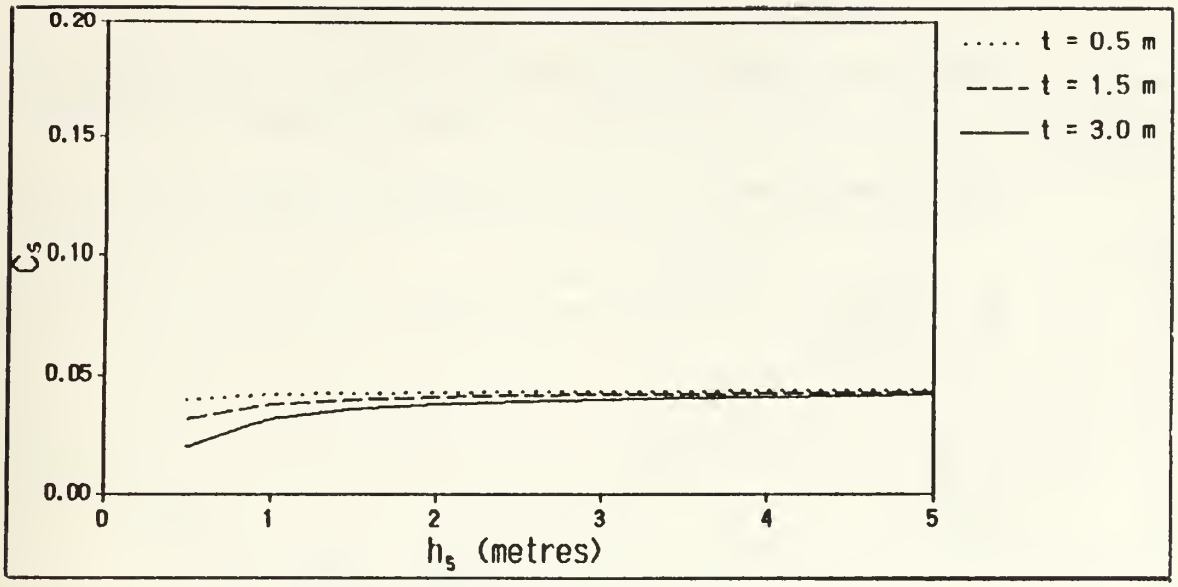

Figure 12. The form coefficient for a pressure ridge sail as a function of sail height and ice sheet thickness.

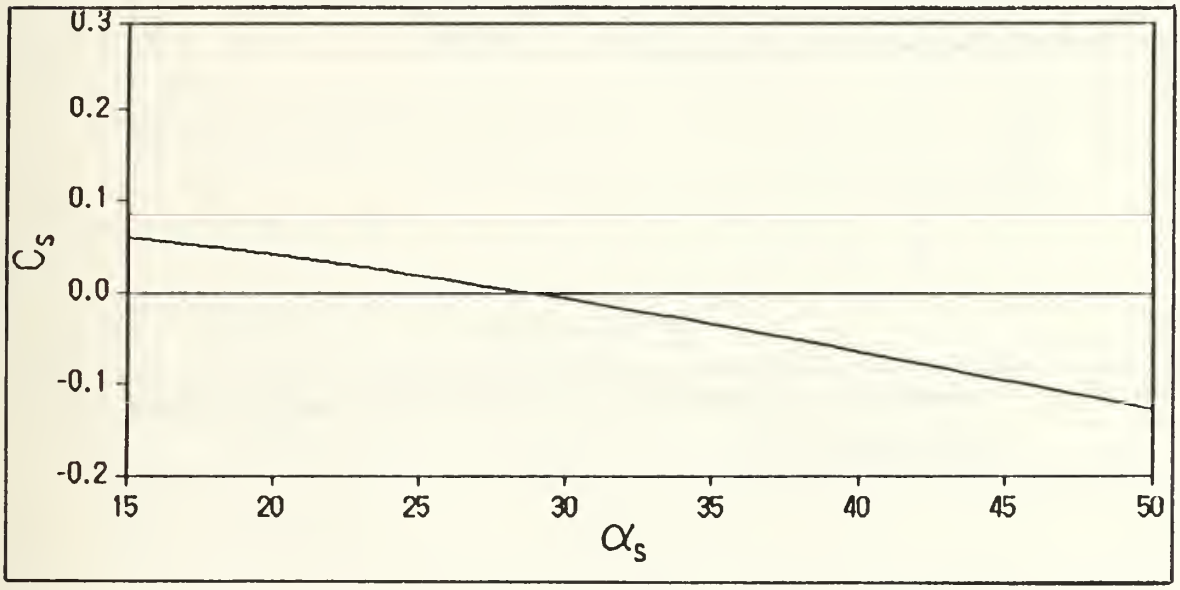

Figure 13. The form coefficient for a pressure ridge sail as a function of sail slope.

c. The Moment Caused by Current Action on the Keel.

The moment M_k caused by the relative current on the keel can be found in a similar way to that found for the sail. The relevant geometry is outlined in Figure 14.

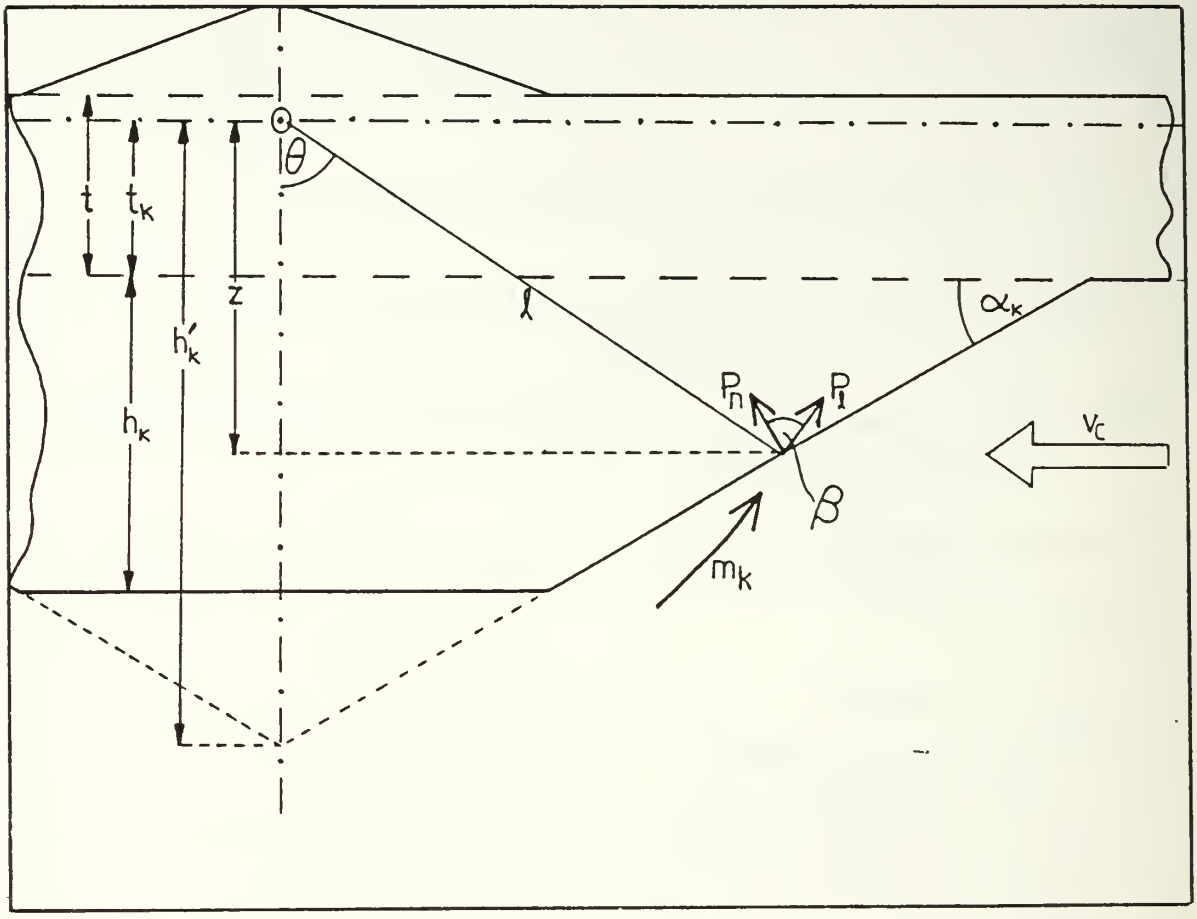

Figure 14. Geometry for calculating the moment caused by relative current on a pressure ridge keel.

By comparison with (21)

$$m_k = \ell P_\ell = \rho_w v_c^2 (h_k' \cos^2\alpha_k - z) \tag{28}$$

Linear current shear is assumed, so

$$v_c(z) = \frac{V_c(z - t_k)}{h_k} \tag{29}$$

$$m_k(z) = \frac{\rho_w V_c^2}{h_k} (z - t_k)^2 (h_k' \cos^2\alpha_k - z) \tag{30}$$

and

$$M_k = \frac{\rho_w V_c^2}{h_k^2} \int_{(h_k + t_k)}^{t_k} (z - t_k)^2 (h_k' \cos^2\alpha_k - z) dz \tag{31}$$

This gives

$$M_k = \frac{\rho_w V_c^2}{12} h_k (4h_k' \cos^2\alpha_k - 3h_k - 4t_k) \tag{32}$$

From (12) $h_k' \simeq 1.7h_k + t_k$, so

$$M_k = \frac{\rho_w V_c^2}{12} (h_k^2 (6.8 \cos^2\alpha_k - 3) + h_k t_k (4 \cos^2\alpha_k - 4)) \tag{33}$$

If $\alpha_s \simeq 30°$ and $t_k \simeq 0.9t$

$$M_k = \frac{\rho_w V_c^2}{12} (2h_k^2 - 0.9h_k t) \tag{34}$$

or

$$M_k = \rho_w V_c^2 h_k^2 C_k \tag{35}$$

where C_k is a form coefficient for the keel given by

$$C_k \simeq \left(163 - 75 \frac{t}{h_k}\right) \times 10^{-3} \tag{36}$$

Figure 15 shows C_k plotted against h_k for various values of t. There is more dependence on t than in the case of C_s and it should be noted that $C_k \simeq 0.15$ for $h_k \gtrsim 1$ m. Also comparing Figures 12 and 15, C_k is generally about four times bigger than C_s. When α_k is increased, there is a point at about 44° where M_k reverses sign as in the case of M_s at greater slopes (see Figure 16). Again this may be relevant when considering relatively new, unweathered, ridges.

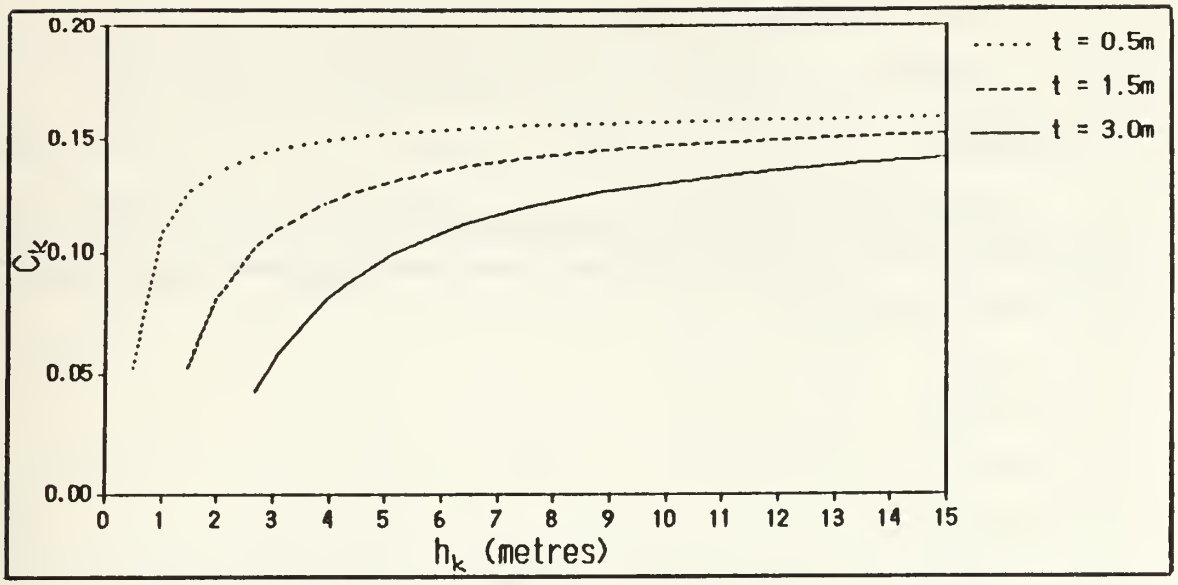

Figure 15. The form coefficient for a pressure ridge keel as a function of sail height and ice sheet thickness.

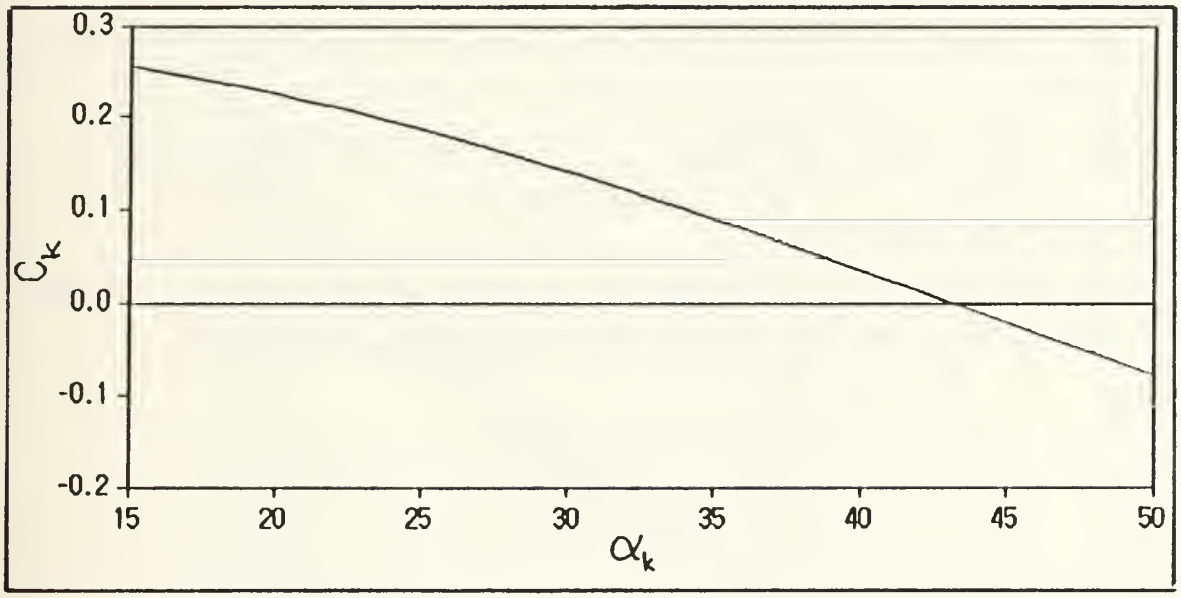

Figure 16. The form coefficient for a pressure ridge keel as a function of keel slope.

The total moment M_a on the ridge structure about point O is given by the sum of the moments caused by wind on the sail and relative current on the keel.

$$M_a = M_s + M_k \tag{37}$$

Figure 17 shows M_a with its constituent components M_s and M_k, as given by (25) and (35), plotted against h, with t = 1.5 m. Typical values for ρ_a, V_w, ρ_w and V_c have been used, they are summarized below:-

$\rho_a = 1.3$ kg m^{-3}

$\rho_w = 1026$ kg m^{-3}

$V_w = 10$ m s^{-1}

$V_c = 0.2$ m s^{-1}

These wind and current velocity values were chosen to represent the upper limits of observed measurements from the literature , i.e., a *worst* case has been chosen in order that the resulting moments will be the largest that could normally be expected to occur in nature.

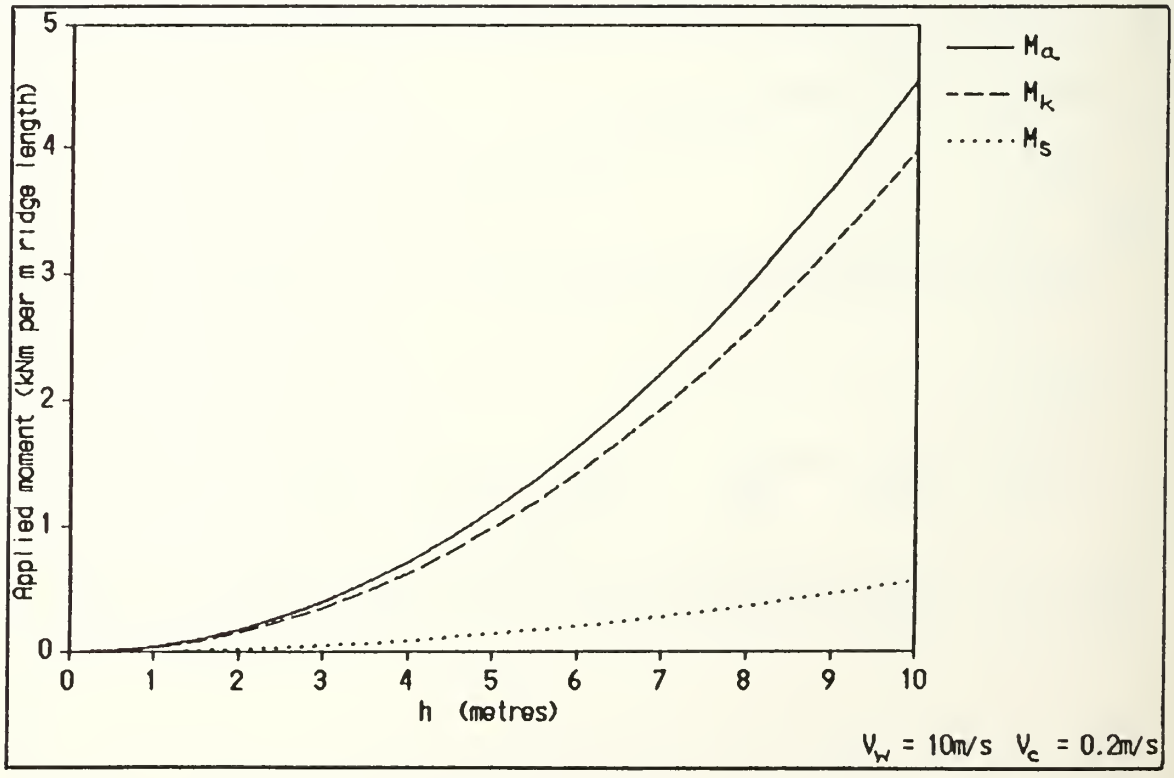

Figure 17. Components of the applied moment at a pressure ridge on 1.5m thick ice (kNm per m ridge length).

Figure 18 is a plot of M_a against t and h_s with $V_w = 10\ \mathrm{m\ s^{-1}}$ and $V_c = 0.2\ \mathrm{m\ s^{-1}}$. The weak dependence on ice sheet thickness is apparent as is the order of magnitude of M_a to be expected for these conditions, i.e., $M_a \sim 1$ kN m per m ridge length.

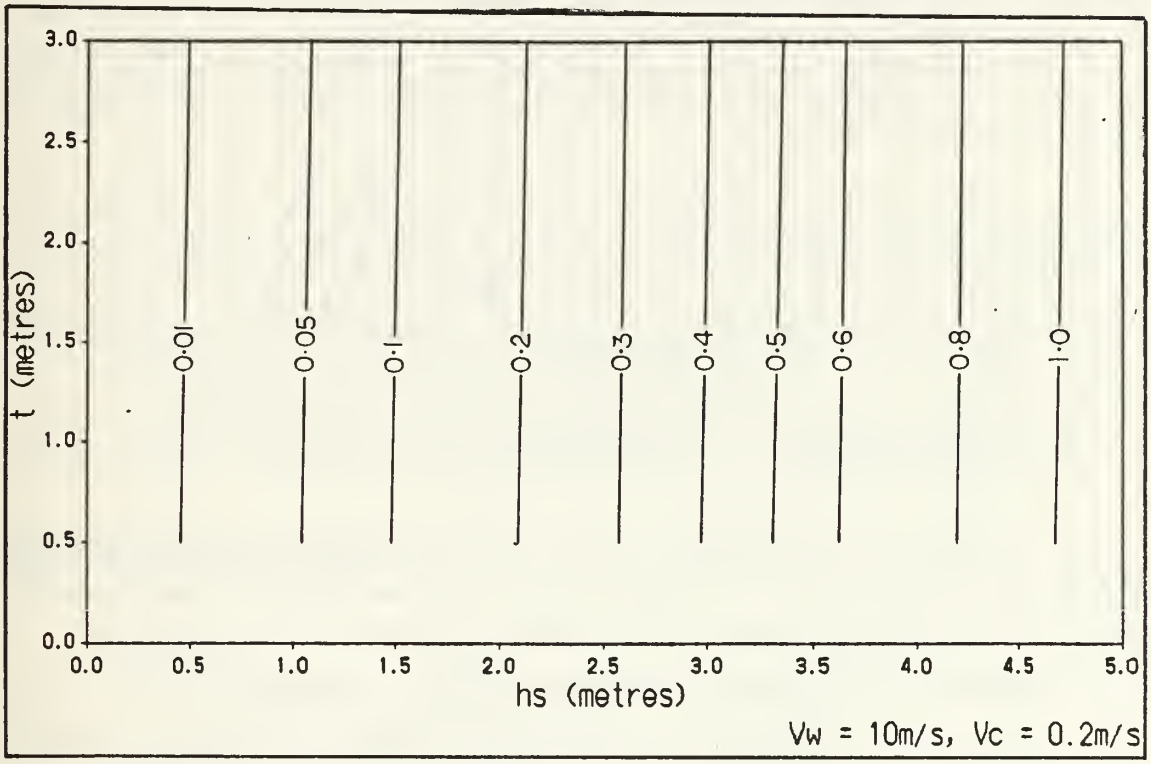

Figure 18. The total moment applied by wind and current at a pressure ridge as a function of sail height and ice sheet thickness (kNm per m ridge length).

The following points arise from the preceding calculation of the moment due to wind and relative current action on a pressure ridge.

1. M_k is the dominant component of M_a.
2. t, the thickness of the ice sheet has little effect on the absolute value of M_a.
3. For angles of slope α_s and α_k taken from Wright et al. (1978) M_a is anticlockwise when the wind blows from the left and the current acts from the right (as shown in Figure 6). If steeper slopes are assumed, M_a could be reversed. Regardless of the sense of the resulting moment, however, the absolute value of M_a at the ridge will be of much the same order.

There are two considerations which have not been taken into account when calculating M_s and M_k which might lead to increased moments at the ridge.

1. The surfaces of both the sail and keel have been assumed smooth. If a more realistic approach were to be taken and some roughness allowed, drag could be expected parallel to the sail and keel surfaces.
2. Reduced pressure in the flow downstream of both the sail and keel would also have some effect on M_s and M_k. This would contribute in a clockwise sense for a wind blowing from the left and current from the right.

Despite these possible inaccuracies and any others which might arise from the assumptions made, equations (25) to (28) and (35) to (37) allow a reasonable estimate of M_a to be made for sensible values of ridge height and ice sheet thickness.

2. The Effect Of An Applied Bending Moment On The Ice Sheet.

In order for the moment M_a, described above, to cause ambient noise under the ice, cracking must occur in the ice sheet. The horizontal distribution of bending moment $M(x)$ on the ice sheet must therefore be investigated in order to estimate the maximum moment that could be expected under normal circumstances. Two extreme cases are examined to determine whether the maximum expected bending moment on the ice sheet is likely to be sufficiently large to cause cracking. The first case examines the ridge as a relatively new feature when it is in an unconsolidated state. That is, it is assumed that the ridge structure consists of loose rubble and ice blocks and therefore contributes no strength to the system. The second case, representing an older pressure ridge, occurs when the ice debris comprising the sail and keel has frozen into a consolidated mass which together with the ice sheet near the ridge can be considered rigid. Figure 19 compares, schematically, the two conditions outlined above.

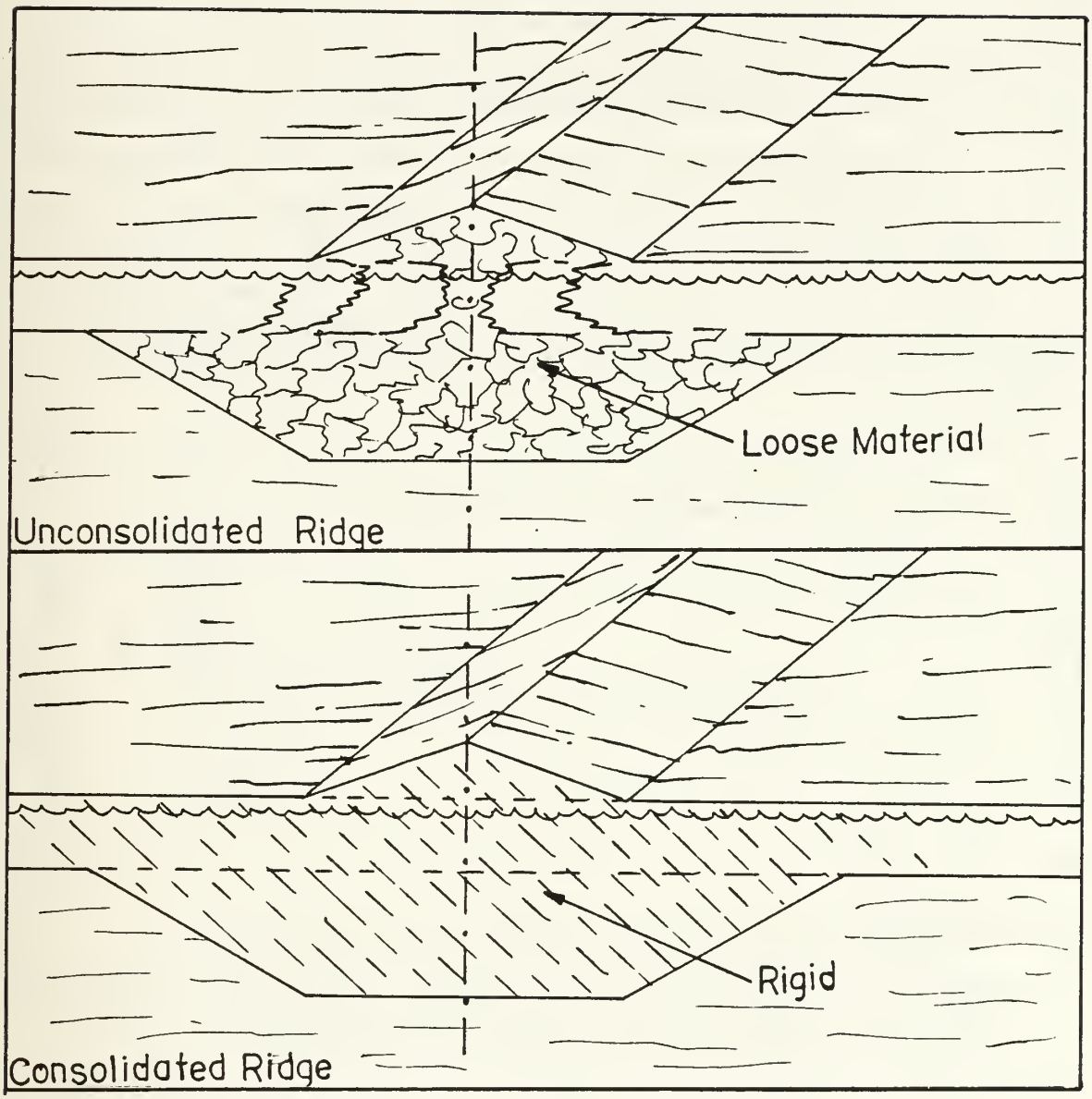

Figure 19. Consolidated and unconsolidated pressure ridges.

a. The Unconsolidated Pressure Ridge.

In this case the ridge ice sheet system is assumed to behave in the same way as two adjoining, loaded, semi-infinite beams on an elastic foundation. The unconsolidated mass of rubble and ice blocks forming the sail and keel interact with the wind and current as described previously to cause an applied moment M_a and also a distributed loading on the ice sheet. They do not however contribute in any way to the strength of the sheet. In order to calculate the expected bending moments on the ice sheet the section to the right of the ridge axis is treated as a semi-infinite beam with static loadings contributed by the sail and keel as shown in Figure 20. The total loading can be thought of as being due to three triangularly distributed loadings. That is, a downward load due to the weight of the ice in the sail (triangle ABC in Figure 20) and an upward loading due to the buoyancy of the keel (triangle DEH minus triangle FGH). So in the isostatic condition

$$y_i(x) = y_{ABC} - y_{DEH} + y_{FGH} \tag{38}$$

where y is the downward displacement of the ice sheet, or

$$y_i(x) = y_{(down)} - y_{(up)} \tag{39}$$

Similarly

$$M_i(x) = M_{ABC} - M_{DEH} + M_{FGH} \tag{40}$$

or

$$M_i(x) = M_{(down)} - M_{(up)} \tag{41}$$

M is the bending moment on the ice sheet (positive in the clockwise direction).

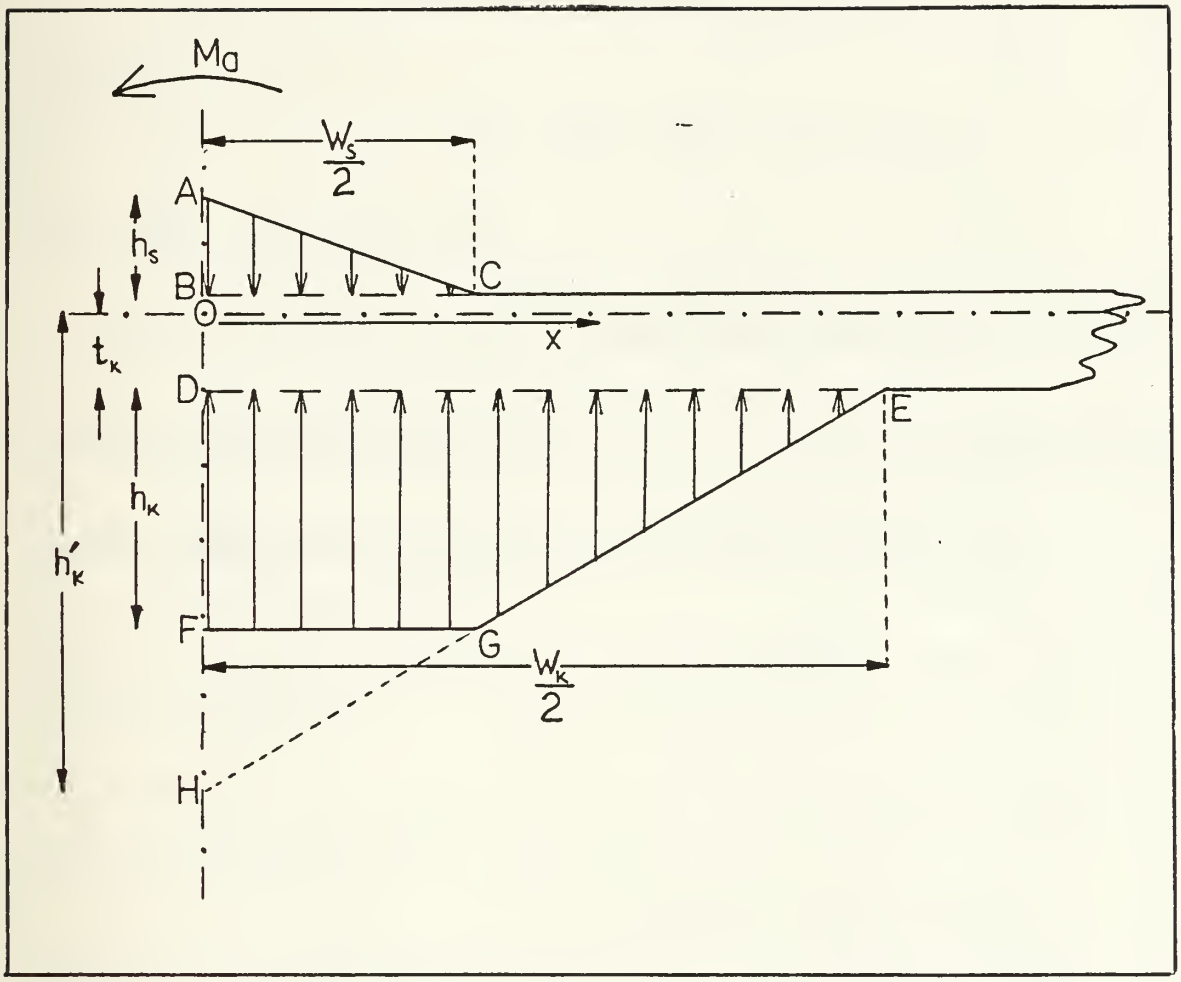

Figure 20. Static loading on the ice sheet by an unconsolidated pressure ridge.

Equations for the displacement and bending moment on a semi-infinite beam subject to triangularly distributed loading have been developed from Hetenyi (1947) in the appendix. They are:-

$$y(x) = q_0 F(\lambda, \ell, x) \qquad 0 \leq x < \ell \quad (42)$$

where $F(\lambda, \ell, x) = (C_{\lambda|\ell-x|} + 4\lambda(\ell - x) + B_{\lambda x}A_{\lambda\ell} - D_{\lambda x}(A_{\lambda\ell} + 2B_{\lambda\ell}))$

$$y(x) = q_0 G(\lambda, \ell, x) \qquad x \geq \ell \quad (43)$$

where $G(\lambda, \ell, x) = (C_{\lambda|\ell-x|} + B_{\lambda x}A_{\lambda\ell} - D_{\lambda x}(A_{\lambda\ell} + 2B_{\lambda\ell}))$ and

$$M(x) = -q_0 H(\lambda, \ell, x) \qquad 0 \leq x \quad (44)$$

where $H(\lambda, \ell, x) = (A_{\lambda|\ell-x|} - D_{\lambda x}A_{\lambda\ell} - B_{\lambda x}(A_{\lambda\ell} + 2B_{\lambda\ell}))$

ℓ is the base length of the triangular loading

and q_0 is the loading at the free end of the beam, i.e., at $x = 0$

see the appendix for definitions of $1/\lambda$ the characteristic length, k the foundation modulus and the functions A_x, B_x, C_x and D_x.

The net downward loading $q_{0(down)}$ is found by considering triangles ABC and FGH (see Figure 20).

$$q_{0(down)} = h_s\rho_i g + (h_k' - h_k - t_k)(\rho_w - \rho_i)g \qquad (45)$$

and using (11) and (6)

$$q_{0(down)} = h_s g(\rho_i + 1.6(\rho_w - \rho_i))$$

Taking $\rho_i \simeq 920$ kg m^{-3} and $\rho_w \simeq 1026$ kg m^{-3}

$$q_{0(down)} = 10670h_s \text{ kg m}^{-1}\text{s}^{-2} \qquad (46)$$

From Figure 20

$$\ell_{(down)} = \frac{W_s}{2} = \frac{h_s}{\tan\alpha_s} \simeq 2.8h_s \qquad (47)$$

For the upward loading $q_{0(up)}$ (due to triangle DEH)

$$q_{0(up)} = (h_k' - t_k)(\rho_w - \rho_i)g \tag{48}$$

$$q_{0(up)} = 4h_s(\rho_w - \rho_i)g$$

or, using the constant values given above

$$q_{0(up)} \simeq 4155h_s \quad \text{kg m}^{-1}\text{s}^{-2} \tag{49}$$

From Figure 20

$$\ell_{(up)} = \frac{W_k}{2} = \frac{h_k}{\tan \alpha_k} + \frac{W_s}{2} \simeq 7h_s \tag{50}$$

Substituting for q_0 and ℓ in (42), (43) and (44), also taking $k = (\rho_w - \rho_i)g \simeq 1039$ kg m^{-2}s^{-2}

$$y_{(down)}(x) = 0.942\, F(\lambda, \ell_{(down)}, x) \qquad 0 \le x < \ell_{(down)} \tag{51}$$

$$y_{(down)}(x) = 0.942\, G(\lambda, \ell_{(down)}, x) \qquad x \ge \ell_{(down)} \tag{52}$$

$$M_{(down)}(x) = -485\, H(\lambda, \ell_{(down)}, x) \qquad 0 \le x \tag{53}$$

$$y_{(up)}(x) = 0.144\, F(\lambda, \ell_{(up)}, x) \qquad 0 \le x < \ell_{(up)} \tag{54}$$

$$y_{(up)}(x) = 0.144\, G(\lambda, \ell_{(up)}, x) \qquad x \ge \ell_{(up)} \tag{55}$$

$$M_{(up)}(x) = -75\, H(\lambda, \ell_{(up)}, x) \qquad 0 \le x \tag{56}$$

Both $\ell_{(up)}$ and $\ell_{(down)}$ are related to h_s by (47) and (50) and λ is a function of t, so from (39)

$$y_i(x) = 0.942\, F_{(down)}(t, h_s, x) - 0.144\, F_{(up)}(t, h_s, x) \qquad 0 \le x < \ell_{(down)} \quad (57)$$

$$y_i(x) = 0.942\, G_{(down)}(t, h_s, x) - 0.144\, F_{(up)}(t, h_s, x) \qquad \ell_{(down)} \le x < \ell_{(up)} \quad (58)$$

$$y_i(x) = 0.942\, G_{(down)}(t, h_s, x) - 0.144\, G_{(up)}(t, h_s, x) \qquad x \ge \ell_{(up)} \quad (59)$$

and from (41)

$$M_i(x) = -485\, H_{(down)}(t, h_s, x) + 75\, H_{(up)}(t, h_s, x) \qquad 0 \le x \quad (60)$$

Figures 21 and 22 show the displacements of ice sheets of various thicknesses when subjected to the loading of unconsolidated ridges with sail heights of 1.5m and 3m. It can be seen that the concentrated mass of the sail causes downward displacement at the ridge axis. The more distributed buoyancy force due to the keel causes upward displacement away from the ridge. This results in bending moment curves as shown by Figures 23 and 24. The value of the constant λ was calculated using a typical value for E, the Young's Modulus for ice. $E = 3 \times 10^9$ Pa, from Mellor (1986).

The absolute value of the bending moment due to the isostatic loading on the ice sheet reaches a maximum value M_{max} some 10 to 20 m from the ridge axis. It is at this point, with or without the additional applied moment M_a due to the wind and relative current, that cracking is most likely to occur. Figure 25 shows M_{max} plotted against h_s and t.

Having established estimates for M_a the applied moment and M_{max} the maximum bending moment on the ice sheet due to isostatic loading, the two can be compared over a range of ridge heights and ice sheet thicknesses. From Figure 18 and Figure 25 it is apparent that M_a is of the order 0 to 1 kN m per m ridge length for realistic maximum wind and current speeds. M_{max}, however, is of the order 20 to 2000 kN m per m ridge length, i.e., M_{max} is roughly two orders of magnitude greater than M_a for a given ridge size.

Thus, it is concluded that if cracking occurs in the unconsolidated case, it will be due almost entirely to the isostatic loading on the ice sheet. The additional applied moment M_a, while not being sufficient to cause cracking by itself, could possibly act as a trigger mechanism for cracking where a cracking event due to isostatic loading was likely to occur anyway.

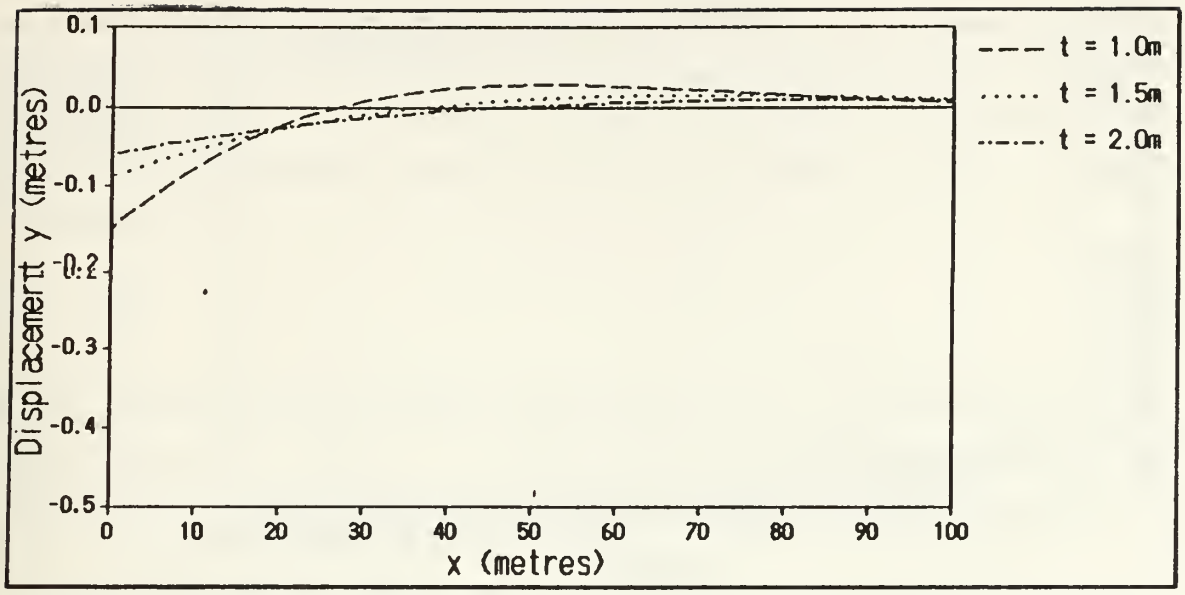

Figure 21. Ice sheet displacement due to isostatic loading of an unconsolidated pressure ridge, height 1.5m.

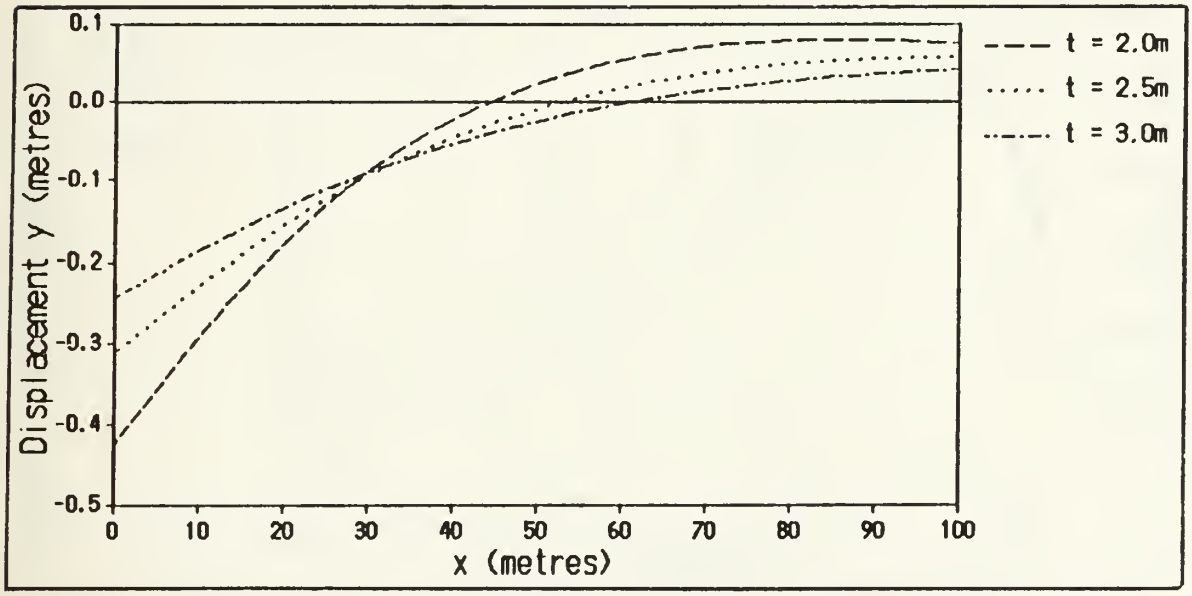

Figure 22. Ice sheet displacement due to isostatic loading of an unconsolidated pressure ridge, height 3.0m.

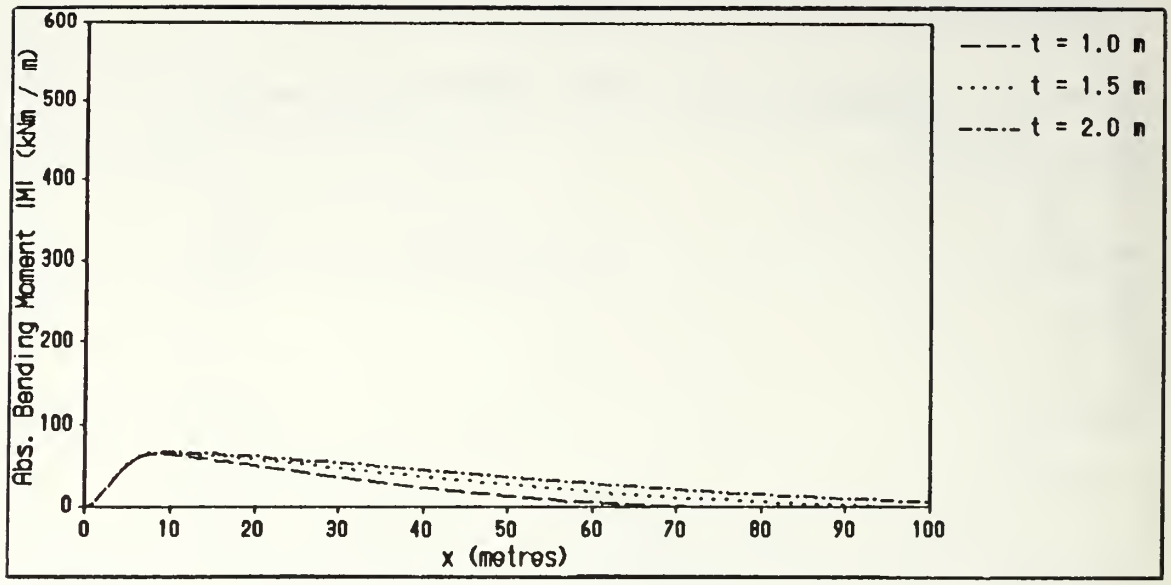

Figure 23. Absolute bending moment on the ice sheet due to isostatic loading of an unconsolidated pressure ridge, height 1.5m.

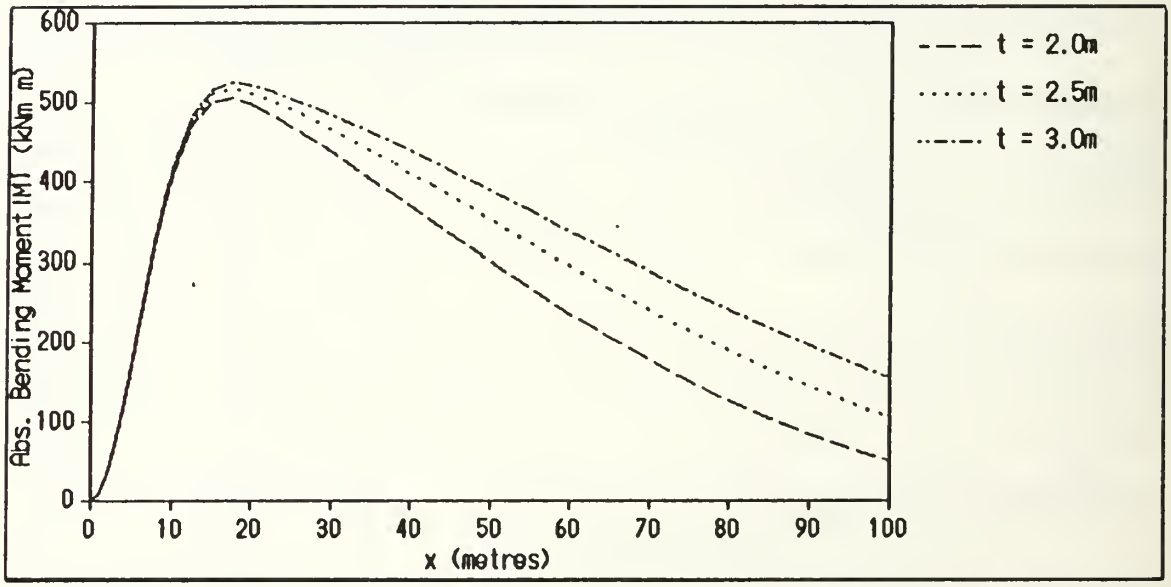

Figure 24. Absolute bending moment on the ice sheet due to isostatic loading of an unconsolidated pressure ridge, height 3.0m.

In order to establish the likelihood of cracking due to isostatic loading alone, M_{max} is compared to the critical bending moment M_{crit} at which cracking will occur. M_{crit} is dependent on σ_t the tensile strength of the ice sheet, and its thickness t. A nominal value for the tensile strength of the ice sheet was taken, $\sigma_t = 0.4 \times 10^6$ Pa from Mellor (1986).

$$M_{crit} = \frac{\sigma_t t^2}{6} \tag{61}$$

Figure 26 shows the ratio M_{max}/M_{crit} plotted against h_s and t. From this graph it can be seen that $M_{max}/M_{crit} \simeq 1$ where $t \sim h_s$. When $M_{max}/M_{crit} \gtrsim 1$ cracking due to isostatic loading is likely to occur. It should be noted that as h_s becomes much greater than t the result is a greater likelihood of cracking.

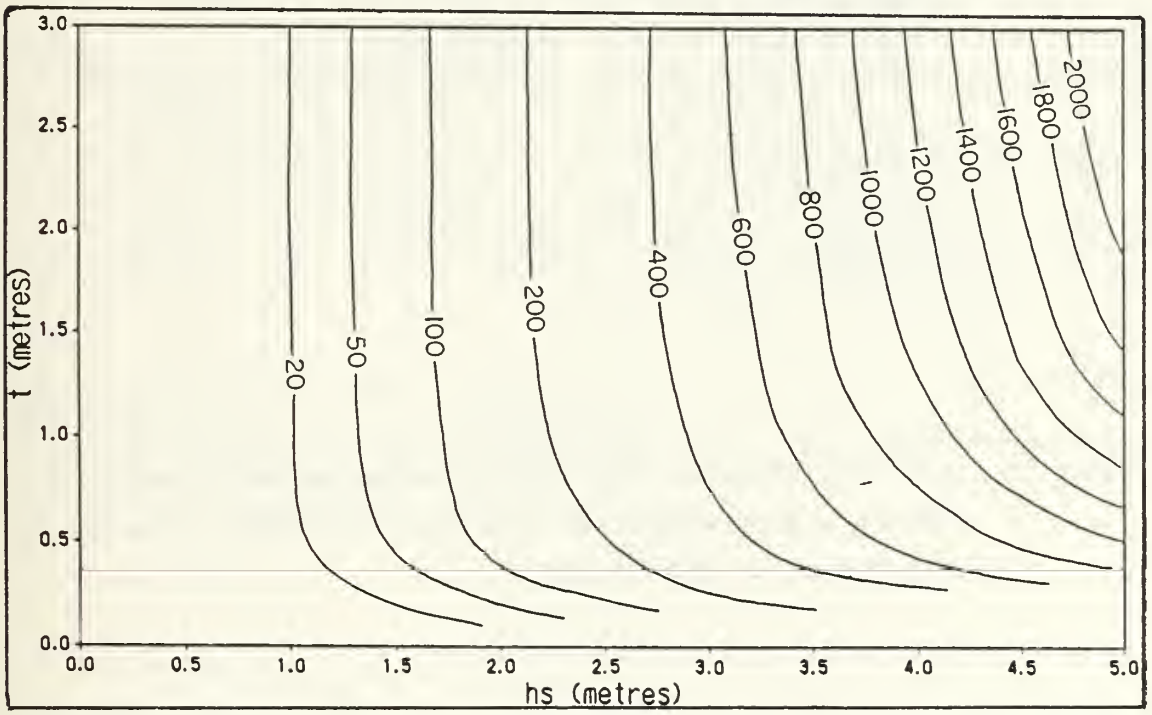

Figure 25. **Maximum bending moment on the ice sheet as a function of sail height and ice sheet thickness (kN m per m ridge length).**

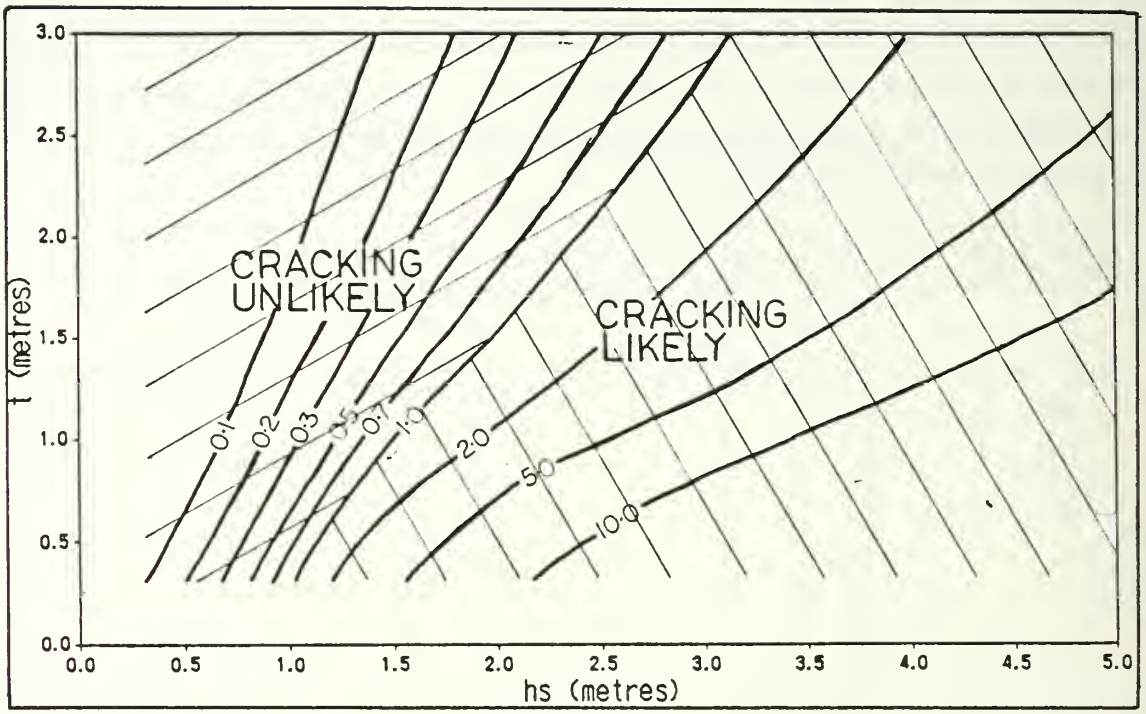

Figure 26. The ratio between maximum bending moment and critical bending moment for an unconsolidated ridge under isostatic loading as a function of sail height and ice sheet thickness.

b. The Consolidated Pressure Ridge.

In this case a completely rigid system is envisaged. It is assumed that the ridge structure has undergone repeated freezing events and is no longer active in that ridge building processes have ceased. The material comprising the sail and keel has frozen into a solid mass and contributes fully to the strength of the ice sheet. The solid ridge section is therefore treated as a rigid beam pivoting about point O (see Figure 27) while the adjoining ice sheets either side of the ridge are assumed to act as semi-infinite beams on elastic foundations. The boundary at section A-A, between the rigid portion (the sail, keel and an unknown length of ice sheet) and the rest of the ice sheet (which is considered flexible), lies a distance L from the ridge axis. Equations for the displacement and slope of a semi-infinite beam on an elastic foundation are taken from Hetenyi (1947) and can be found in the appendix.

For simplicity, symmetry about the ridge axis is assumed such that

1. The distances L_L and L_R equal.
2. y_L and y_R, the displacements of the ice sheet at distances L either side of the ridge axis, are equal and opposite.
3. M_L and M_R, the bending moments on the ice sheet at distances L either side of the ridge axis, are equal and opposite.
4. Q_L and Q_R, the shear forces at distances L either side of the ridge axis, are equal and opposite.

Thus

$$L_L = -L_R = -L$$

$$y_L = -y_R = y$$

$$M_L = -M_R = M$$

and

$$Q_L = -Q_R = Q$$

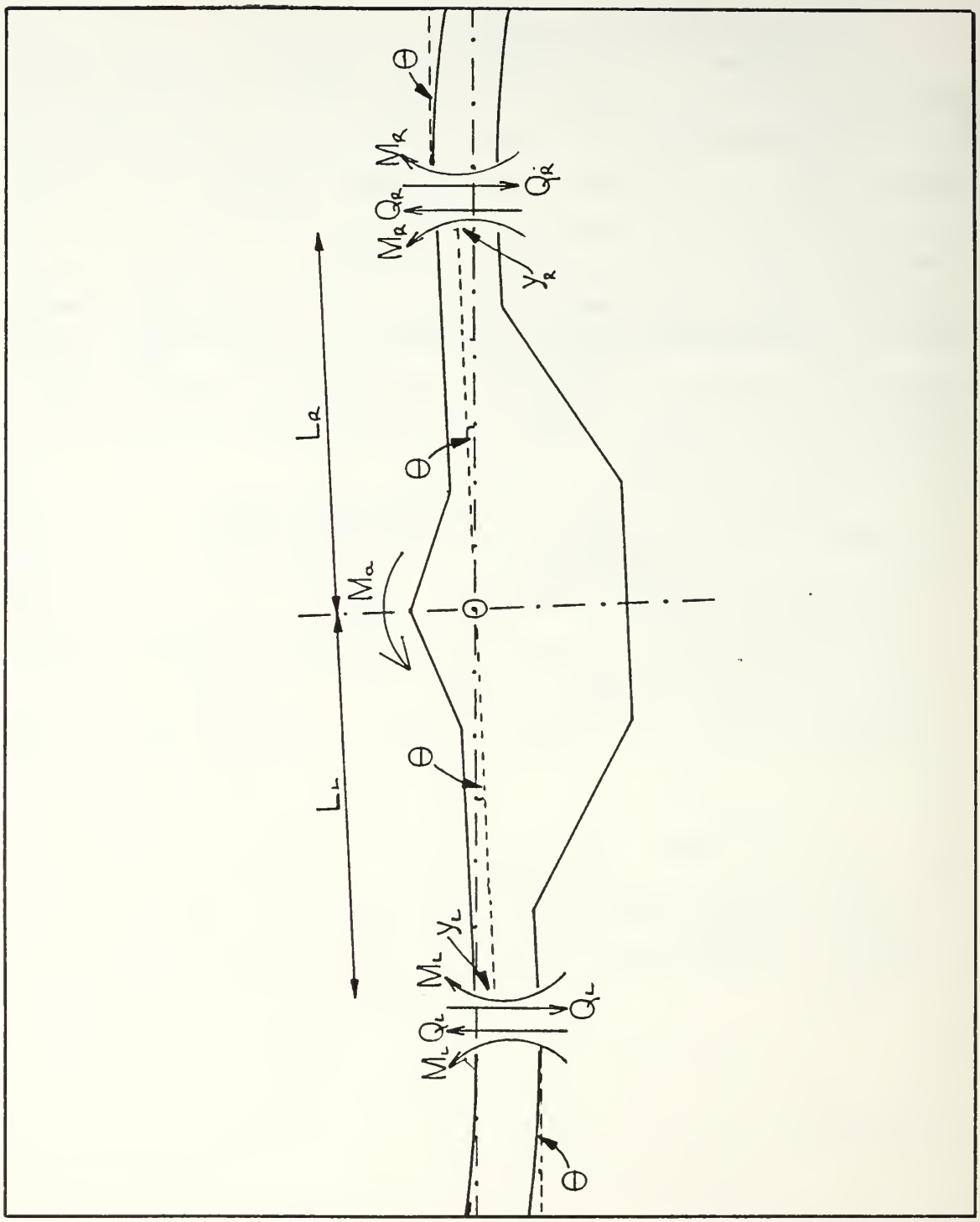

Figure 27. Geometry and general structure of the consolidated pressure ridge model.

Now summing the moments about point O

$$\Sigma M_0 = M_b + M_L - M_R - LQ_L - LQ_R - M_a = 0$$

or given the assumption of symmetry above

$$M_b + 2M + 2LQ = 0 \tag{62}$$

M_b is the moment caused by the immersion of ice to the left of O and emmersion of ice to the right.

$$M_b = \int_{-L}^{L} x^2 k \tan\theta \, dx \quad = 2/3kL^3 \tan\theta$$

or

$$M_b \simeq 2/3kL^3\theta \quad \text{for small } \theta \tag{63}$$

From the appendix, the displacement of a semi-infinite beam subjected to a shear force Q and moment M at its free end is given by

$$y = \frac{2Q\lambda}{k} D_{\lambda x} - \frac{2M\lambda^2}{k} C_{\lambda x}$$

See the appendix for definitions of $1/\lambda$ the characteristic length, k the foundation modulus and the functions A_x, B_x, C_x and D_x . Since the section A-A, distance L from the ridge axis, coincides with the begining of the flexible ice sheet and therefore the free end of the semi-infinite beam model, $x = 0$ and $D_{\lambda x} = C_{\lambda x} = 1$. Therefore

$$y = \frac{2Q\lambda}{k} - \frac{2M\lambda^2}{k} \quad = \quad \frac{2\lambda}{k}(Q - M\lambda) \tag{64}$$

The slope θ of the semi-infinite beam section is also given in terms of Q and M in the appendix.

$$\theta = -\frac{2Q\lambda^2}{k} A_{\lambda x} + \frac{4M\lambda^3}{k} D_{\lambda x}$$

Again at the free end $x = 0$ so $A_{\lambda x} = D_{\lambda x} = 1$

$$\theta = -\frac{2Q\lambda^2}{k} + \frac{4M\lambda^3}{k} = \frac{2\lambda^2}{k}(2M\lambda - Q) \tag{65}$$

Also, from Figure 27

$$\tan\theta = \frac{y}{L} \text{ or } y = \theta L \text{ for small } \theta \tag{66}$$

Now subsituting (63) and (65) into (62)

$$\frac{4}{3} L^3\lambda^2(2M\lambda - Q) + 2m + 2LQ - M_a = 0 \tag{67}$$

and from (64), (65) and (66)

$$Q = \frac{M\lambda(1 + 2\lambda L)}{(1 + \lambda L)} \tag{68}$$

so (67) becomes

$$M(\frac{4}{3}(\lambda L)^3 + 4(\lambda L)^2 + 4(\lambda L) + 2) - M_a(1 + (\lambda L)) = 0$$

The effect of the applied moment M_a on M, the bending moment at the interface region between the rigid pressure ridge section and the flexible ice sheet, is therefore given by

$$\frac{M}{M_a} = \frac{(1 + (\lambda L))}{(\frac{4}{3}(\lambda L)^3 + 4(\lambda L)^2 + 4(\lambda L) + 2)} \tag{69}$$

Figures 28 and 29 show the ratio M/M_a plotted for sail heights of 2 m and 4 m with various ice sheet thicknesses. λ has been calculated using a Young's Modulus of $E = 3 \times 10^9$ Pa and wind and current speeds of 10 m s^{-1} and 0.2 m s^{-1} have again been assumed to represent a *worst case*.

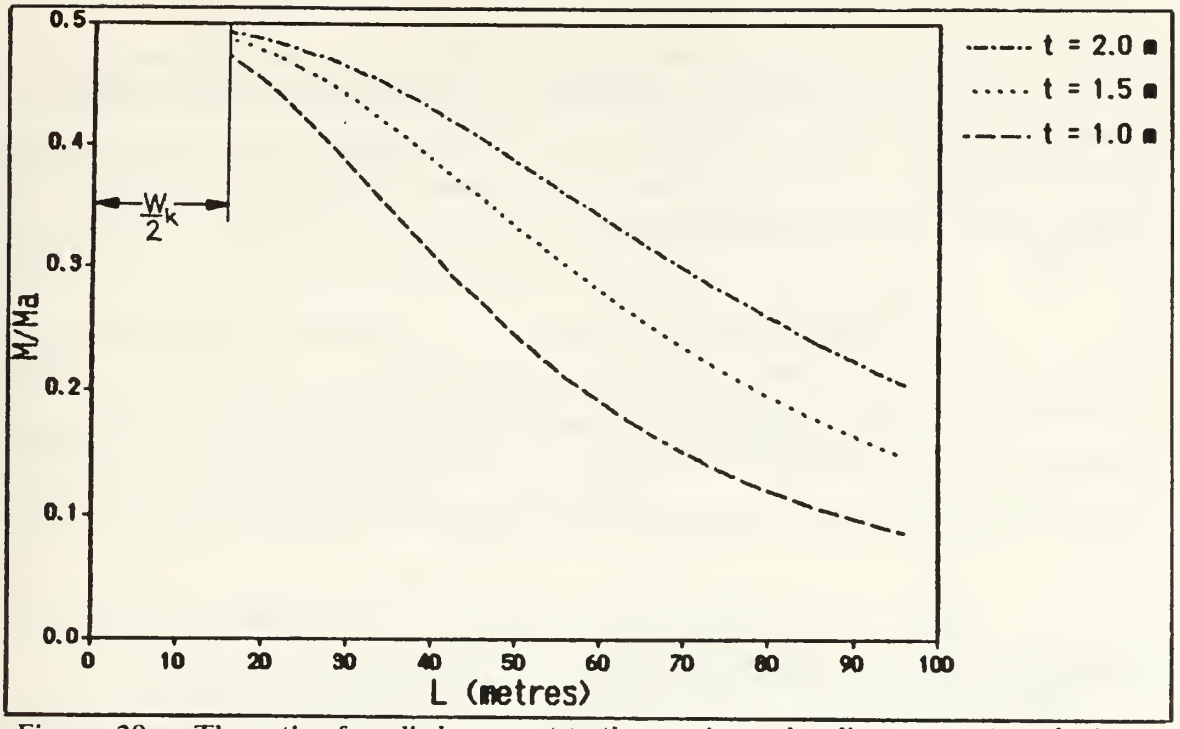

Figure 28. The ratio of applied moment to the maximum bending moment on the ice sheet for a consolidated pressure ridge, height 2m.

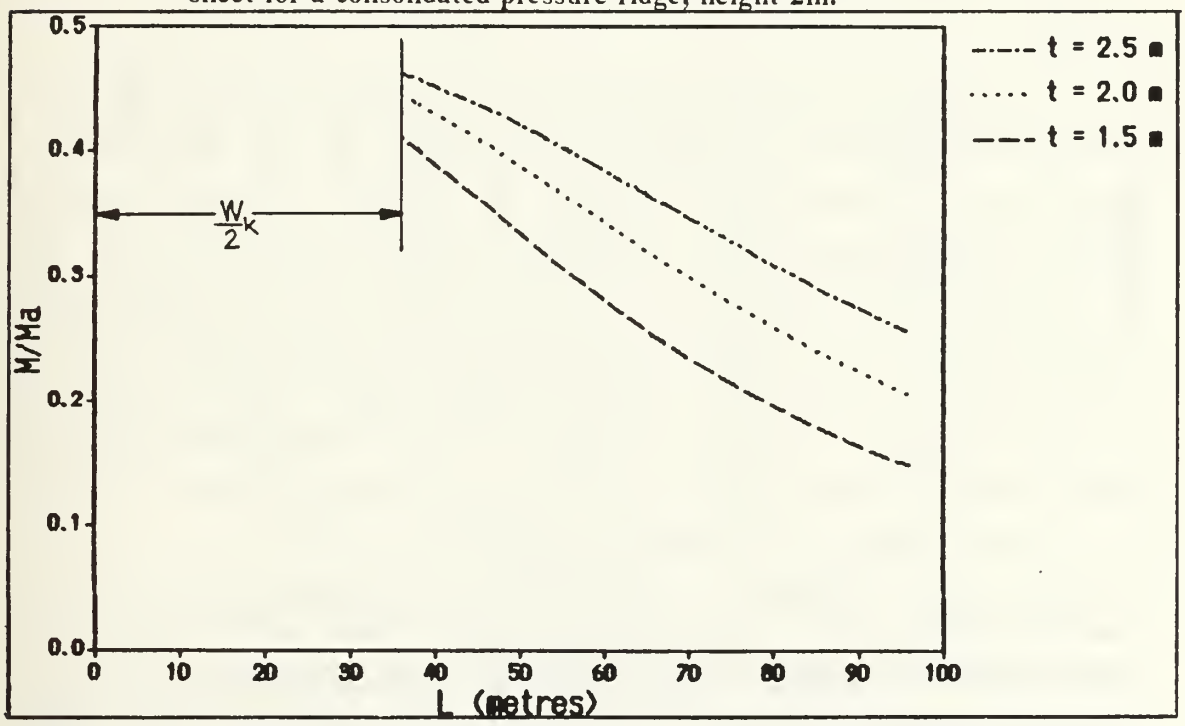

Figure 29. The ratio of applied moment to the maximum bending moment on the ice sheet for a consolidated pressure ridge, height 4m.

Note that (69) is not valid for $L < \frac{W_k}{2}$ since the keel and/or the sail structures significantly increase the rigidity there. It is assumed that cracking is unlikely within the ridge structure itself due to its increased thickness and strength. From Figure 29 the maximum bending moment on the ice sheet itself appears to occur where $L = \frac{W_k}{2}$.

The maximum bending moment M_{max} is plotted for various values of sail height and ice sheet thickness in Figure 30. Note that M_{max} is of the order 0 to 0.5 kN m per metre of ridge length. Comparing this with M_{crit}, the bending moment required for cracking to occur as illustrated by Figure 31, the bending moment available is about three orders of magnitude smaller than that required for cracking to occur in the ice sheet.

Thus, it is concluded that cracking noise is unlikely to occur due to wind/current induced moments applied to a consolidated pressure ridge.

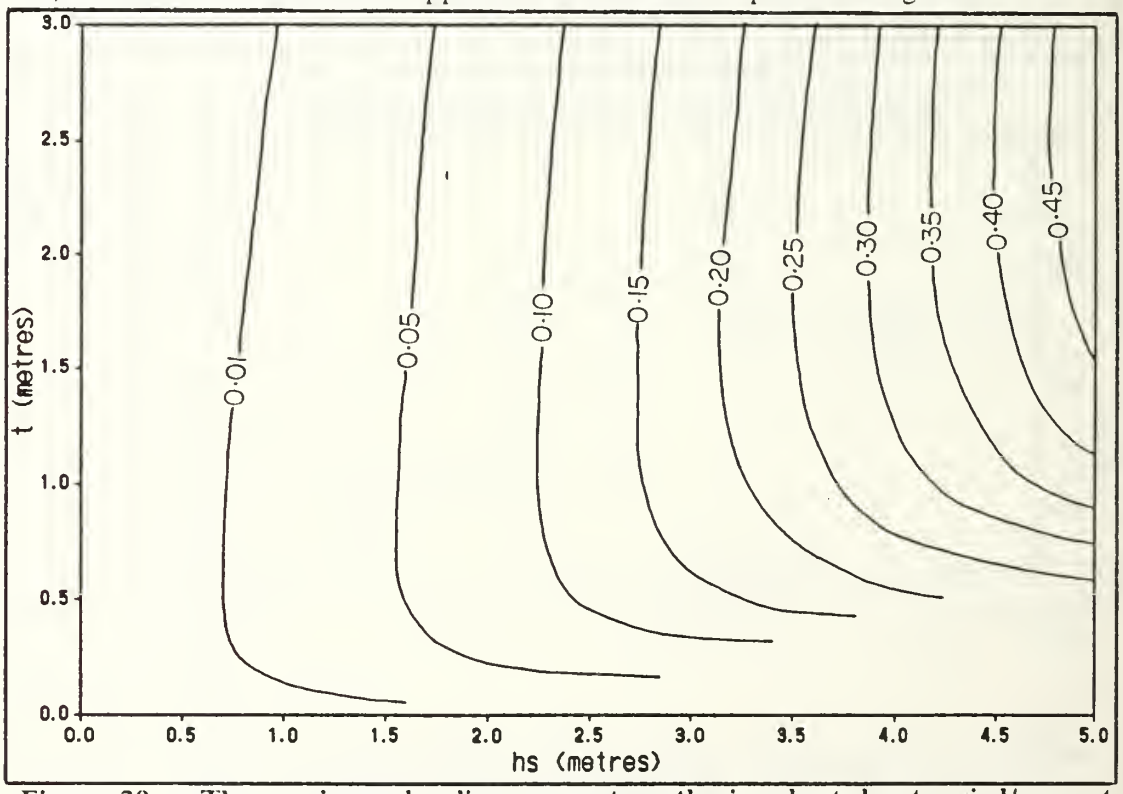

Figure 30. The maximum bending moment on the ice sheet due to wind/current-induced moments at a consolidated pressure ridge (kN m per m ridge length).

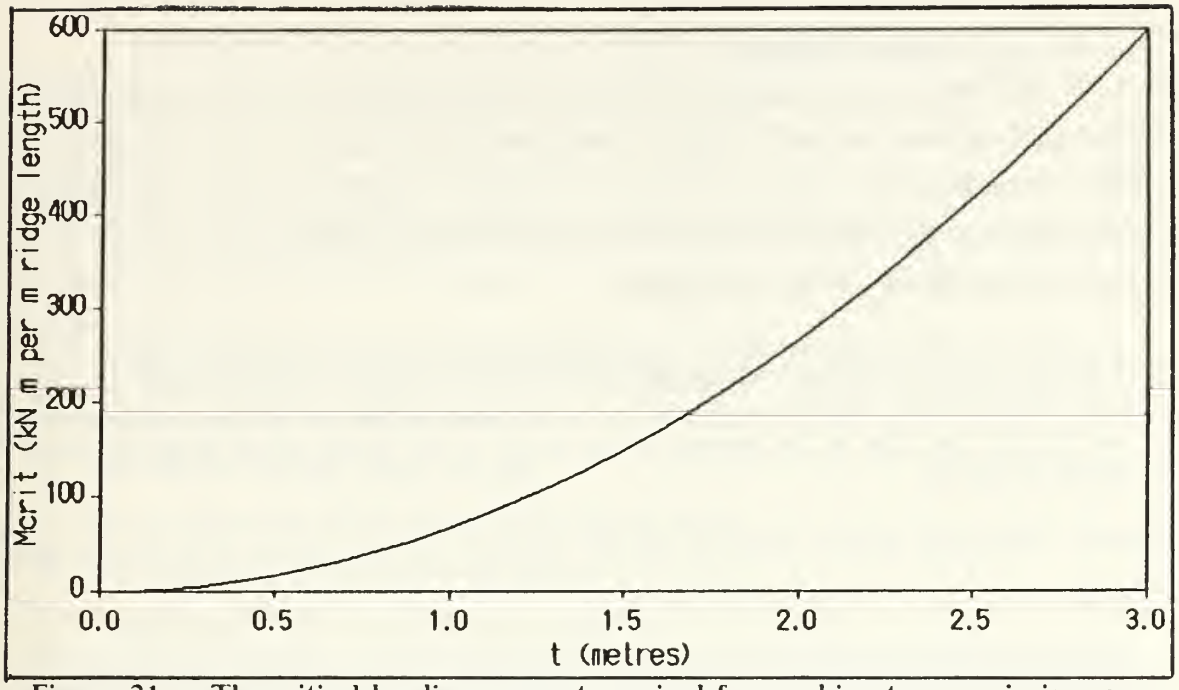

Figure 31. The critical bending moment required for cracking to occur in ice as a function of thickness (kN m per m ridge length).

3. Conclusions : Cracking Noise Due to Wind/Current-Induced Moments.

From the results of a) and b) above it is apparent that the generation of noise due to these processes is unlikely to be of any major significance, if it occurs at all in nature. In the case of the young, unconsolidated, pressure ridge it appears that the bending moments on the ice sheet due to the isostatic loading of the sail and keel structures far outweigh any additional bending moments caused by the effects of wind and current on the ridge. Any cracking which occurs is likely to be due to these loadings. An additional contributor to local ice sheet bending might also be large scale ice stress. This has not been considered here as it would probably be small if the ice were in wind driven motion. There remains the remote possibility that the cracking of heavily loaded ice sheets could be triggered by the onset of wind/current-induced effects. It seems unlikely however that this could account for any significant correlation between wind, current and ambient noise in field measurements. The results of the investigation into the more mature consolidated pressure ridge reveals even less probability of cracking due to wind/current induced bending moments. The strength of the ice is such that it is very unlikely to yield to the relatively weak bending moments so induced. This conclusion is supported by the fact that significant noise levels have never been observed emanating from old inactive pressure ridge features.

4. Ice Fragment Bumping.

This mechanism embraces all the bumping and grinding noises which would be expected to occur when ice fragments move about under an ice sheet. The probability that this mechanism is responsible for the creation of significant levels of ambient noise is reinforced by the recorded observation of audible sounds from the ice surface. Zubov (1943) quotes Weyprecht as stating that

> Sometimes shift at the bottom [of the ridge keel] is audible, with the complete repose of the ice at the top. This occurs probably as a result of the movement of water under the ice field. The difference of the movements of the ice field and of the water on which it lies, that is, the current of the water, is that power which levels the lower depth of the ice.

Zubov (1943) also quotes Makarov on the existence and movement of ice blocks under the ice

> During the third Winter, a fissure was formed under the strip under the *Fram*. The fissure opened, lumps of significant size began to float out from below. "This shows", says Makarov, "that many lower lumps constantly travel. The current of the water and the movement of the ice change their direction so that the migrating ice block stops under certain conditions, under others it can move from the spot."
>
> It is neccessary to add that the lumps which compose the under-ice part of the hummocks [ridges] are not only transformed but are also gradually destroyed.

Ice blocks or fragments are most likely to be the products of active ridging events. In the previous section the behaviour of young unconsolidated ridges was examined quantitatively. The downward depression of material at the ridge axis was shown in Figures 21 and 22. This fractured ice appears to be thrust downward and trapped in buoyant equilibrium under the ice sheet by the ridging processes. Buck and Wilson (1986) describe the forcing of ice blocks as large as four metres thick into the water column in their study of an active pressure ridge.

It is reasonable then that given ice sheet motion relative to the water body below, the loose material will move horizontally. Indeed, further observations by Makarov, (Zubov, 1943) suggest that this is the process by which pressure ridge keels become vertically truncated and more widely spread in the horizontal than the corresponding sail formations.

Given then that there are large ice fragments in motion along the rough under surface of an ice sheet, collisions, grinding and bumping are certain to occur. Noise from this source would probably be similar in nature to that observed as a result of floe-floe interactions in the marginal ice zone. Predominant frequencies are in the range 10 Hz to 1 KHz according to Diachok and Winokur (1974). Certainly the impactive nature of the processes and the variety of fragment sizes is likely to yield noise spread over a wide frequency range.

The intensity and perhaps the frequency range of ambient noise caused by this mechanism would be dependent on

1. The relative current under the ice.
2. The proliferation of ice debris under the ice sheet.
3. The roughness of the under-ice surface.
4. The thickness and density of the ice sheet.

The current strength is of prime importance and is directly related to the translational speed of the ice and or oceanic or tidal currents. The presence of debris and ice roughness are both a function of the deformation history of the ice field and are likely to vary by region. Item 4 has been included as these factors are almost certain to have a bearing on the nature of the sound resulting from impactive events and its propagation into the sea.

Modelling this mechanism is likely to be a complex task if approached from a purely physical standpoint. A more profitable approach might be to seek empirical relationships between the factors outlined above and measured ambient noise levels. This could be backed up by some simple field experiments involving perhaps acoustic monitoring of ice blocks pushed through bore holes.

B. FLOW MECHANISMS.

The potential noise creation mechanisms falling into this category are all driven exclusively by the interaction of the sea with the underside of the ice sheet floating at the surface. The factors important in their operation are therefore the flow velocity of the water relative to the ice, the characteristics of the under-ice surface including cavity shapes and sizes, the roughness, and to some extent the thickness, of the ice cover.

It seems intuiuively obvious that some noise, no matter how small, must be produced when water flows under rough ice. The object here is to explore the mechanisms which may be responsible for this flow noise and assess their importance in the overall generation of ambient noise in an ice covered environment.

Because of the complexity of the mechanisms outlined in this section, involving as they do, turbulent flow over largely random surfaces, the prediction of the noise fields created is somewhat crude. Some of the physical processes are currently being researched and many of the concepts are still only poorly understood (Ross, 1987). Where possible, estimates are made of likely sound characteristics in terms of frequency and intensity. These estimates are based on objective considerations but must be assumed accurate only to an order of magnitude.

A typical composite Arctic ambient noise spectrum is presented in Figure 32. This serves to indicate the intensities required in order for a particular mechanism to be considered important as a contributor. It is probable that flow noise, whether or not it is found to be a significant component of the total noise under pack-ice, would be entirely masked by noise from other mechanisms at locations near the ice edge. For this reason, the measured spectrum chosen to represent the norm is from a central arctic pack-ice location. It is reproduced from Makris and Dyer (1986) who made measurements at 83°*N* 20°*E* in April 1982.

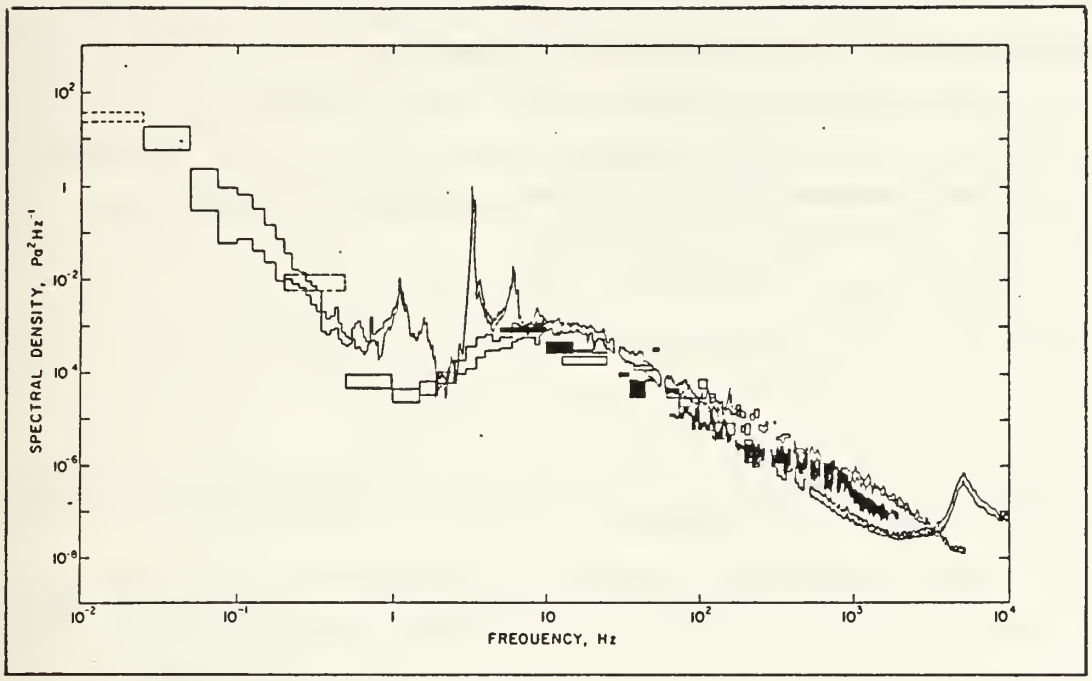

Figure 32. A typical under-ice noise spectrum (from Makris & Dyer, 1986).

1. Noise From the Turbulent Boundary Layer.

a. Boundary Layer Characteristics.

The ratio of kinetic to viscous forces in a flow regime is described by the Reynolds number for that flow.

$$Re = U_0 \frac{L}{\nu} \tag{70}$$

where

U_0 is the free flow velocity beyond the influence of boundaries

L is the length scale associated with the flow

ν is the kinematic viscosity of the fluid = 1.79×10^{-6} m^{-2}s for water at 1 atmosphere and 0°C.

Whenever the Reynolds number exceeds a limiting value the flow becomes unstable and turbulence results. The instability is caused by the dominance of kinetic forces in the flow over viscous forces. For flow under ice, where relative current velocities can be of the order 0.1 to 0.2 m s and length scales measured in thousands of metres, Reynolds numbers can easily exceed 2000, a typical limit for the onset of turbulent flow.

In the presence of a rigid boundary, which in the first approximation can be considered flat and smooth, a turbulent boundary layer is formed. The thickness δ of this boundary layer is a function of the Reynolds number for the flow (White ,1986) such that

$$\frac{\delta}{x} \simeq \frac{0.16}{Re^{1/7}} \tag{71}$$

where

x is the downstream distance from the begining of the boundary which is analagous to the length scale L for ice sheet cover.

If the boundary layer under the ice cover is fully turbulent it can be considered identical to the mixed layer in terms of constant temperature distribution. Thus a typical value of 30 m, representative of arctic mixed layer depths, can be taken for δ the boundary layer depth. It is accepted that processes other than turbulence in the horizontal flow contribute to mixing in the boundary layer under ice but the analogy is presented as a first approximation. From (70) and (71)

$$L = x \simeq \left(\frac{U_0}{\nu}\right)^{1/6}\left(\frac{\delta}{0.16}\right)^{7/6} \tag{72}$$

$$\simeq 3000\text{m for } U_0 = 0.2\text{m s}^{-1} \text{ and } \delta = 30\text{m}$$

This confirms that a rough length scale of the order of thousands of metres with a boundary layer depth of about 30 m is reasonable for large smooth ice sheets in wind driven motion.

b. Noise Mechanisms in the Turbulent Boundary Layer.

Vecchio & Wiley (1973) identified two mechanisms by which noise could be radiated from a turbulent boundary layer. The first is called ***Flow-Induced*** noise and involves acoustic dipoles induced in the boundary by turbulent pressure fluctuations. The second is called ***Flow-Excited*** noise and depends on the elastic behaviour of the boundary which, when excited by turbulent pressure fluctuations, radiates energy back into the fluid.

The direct effect of the pressure fluctuations themselves, set up by turbulent motion in the boundary layer and often referred to as ***Psuedo-Sound*** or ***Quasi-Sound***, could also be considered as a noise producing mechanism in its own right. Pseudo-sound is a non-radiating phenomena, it's direct effect only being felt when pressure fluctuations impinge directly on the active face of a hydrophone. It is closely related to self-noise but is considered here to be purely a product of the turbulent flow and not dependent on hydrophone characteristics.

Since the first two mechanisms mentioned above depend on the presence of pseudo-sound this phenomena will be examined first, both as a driving force for the other mechanisms and as a source of noise in itself.

2. Pseudo-Sound.

a. The Smooth Boundary Approximation.

Skudrzyk and Haddle (1960) describe the length scales of turbulent motion in the boundary layer as varying between the thickness of the boundary layer and the Kolmogorov microscale some 40 times smaller. Patches of turbulence are envisaged passing over a hydrophone or presumably any given point on the boundary at a rate U_c. This is the convection velocity which is proportional to U_0 the free flow velocity such that $U_c \simeq 0.8U_0$. The characteristic frequency f_0 of the resulting pseudo-sound pressure fluctuations is therefore given by

$$f_0 \simeq \frac{U_c}{d} \simeq 0.8\frac{U_0}{d} \tag{73}$$

where

d is the separation between the patches of turbulence being convected past a given point.

If d is approximately equal to the boundary layer depth δ

$$f_0 \simeq 0.8 \frac{U_0}{\delta} \tag{74}$$

Thus, $f_0 \simeq 0.007$ Hz for $U_0 = 0.2$ m s^{-1} and $\delta = 30$ m

Skudrzyk and Haddle (1960) found that the power spectrum of pseudo-sound pressure per unit frequency is virtually constant for frequencies up to f_0 and then decreases inversely proportional to a power m, at frequencies greater than f_0. At $f = f_0$ the pressure due to pseudo-sound is given by

$$p_0^2 = 0.75 \times 10^{-5} \alpha^2 \rho_w^2 U_0^3 \delta^* \frac{3}{2} (m - 1/m) \quad \text{Pa}^2 \tag{75}$$

where

α is the Kraichnan constant

U_0 is the free stream velocity

δ^* is the displacement thickness of the boundary layer $\simeq \delta/5$

ρ_w is the water density

So the power spectrum for pseudo-sound is given by

$$P(f) = 1.5 \times 10^{-6} \alpha^2 \rho_w^2 U_0^3 \delta \frac{3}{2} (m - 1/m) \quad \text{Pa}^2\text{Hz}^{-1} \qquad f \leq f_0 \tag{76}$$

and

$$P(f) = 1.5 \times 10^{-6} \alpha^2 \rho_w^2 U_0^3 \delta \frac{3}{2} (m - 1/m) (f_0/f)^m \quad \text{Pa}^2\text{Hz}^{-1} \qquad f > f_0 \tag{77}$$

α is related to the Reynolds number for the flow and lies between about 0.7 and 6, also Skudrzyk & Haddle (1960) give $m \simeq 3$. Therefore, for water with $\rho_w = 1026$ kg m^{-3}

$$P(f) = 1.6 U_0^3 \alpha^2 \delta \quad \text{Pa}^2\text{Hz}^{-1} \qquad f \leq f_0 \tag{78}$$

and

$$P(f) = 1.6 U_0^3 \alpha^2 \delta (f_0/f)^3 \quad \text{Pa}^2\text{Hz}^{-1} \qquad f > f_0 \tag{79}$$

Lotsch (1971) gives an alternate formula for the pseudo-sound power spectrum in terms of the Strouhal number S

$$P(f) = 3.16 \times 10^{-5} \rho_w^2 \delta^* U_0^3 (1 + (\pi S)^2)^{-3/2} \quad \text{Pa}^2\text{Hz}^{-1} \tag{80}$$

where

$$S = \frac{f\delta^*}{U_0}$$

or taking $\delta^* \simeq \frac{\delta}{5}$ and $\rho_w = 1026\ \text{kg m}^{-3}$

$$P(f) = 6.7\delta U_0^3 \left(1 + \left(\frac{f\pi\delta}{5U_0}\right)^2\right)^{-3/2} \quad \text{Pa}^2\text{Hz}^{-1} \tag{81}$$

Pressure fluctuations or pseudo-sound could affect a hydrophone located in the turbulent boundary layer and be recorded as noise. The estimated spectra, as given by (78) and (79) or (81), when compared to the measured spectrum from Makris and Dyer (1986) show that pseudo-sound is probably insignificant as a noise source if the under side of the ice is smooth (see Figure 33). Although the slope of the roll-off with increased frequency fits well with the measured data, the overall intensity is too small compared with the measured spectrum below 1 Hz.

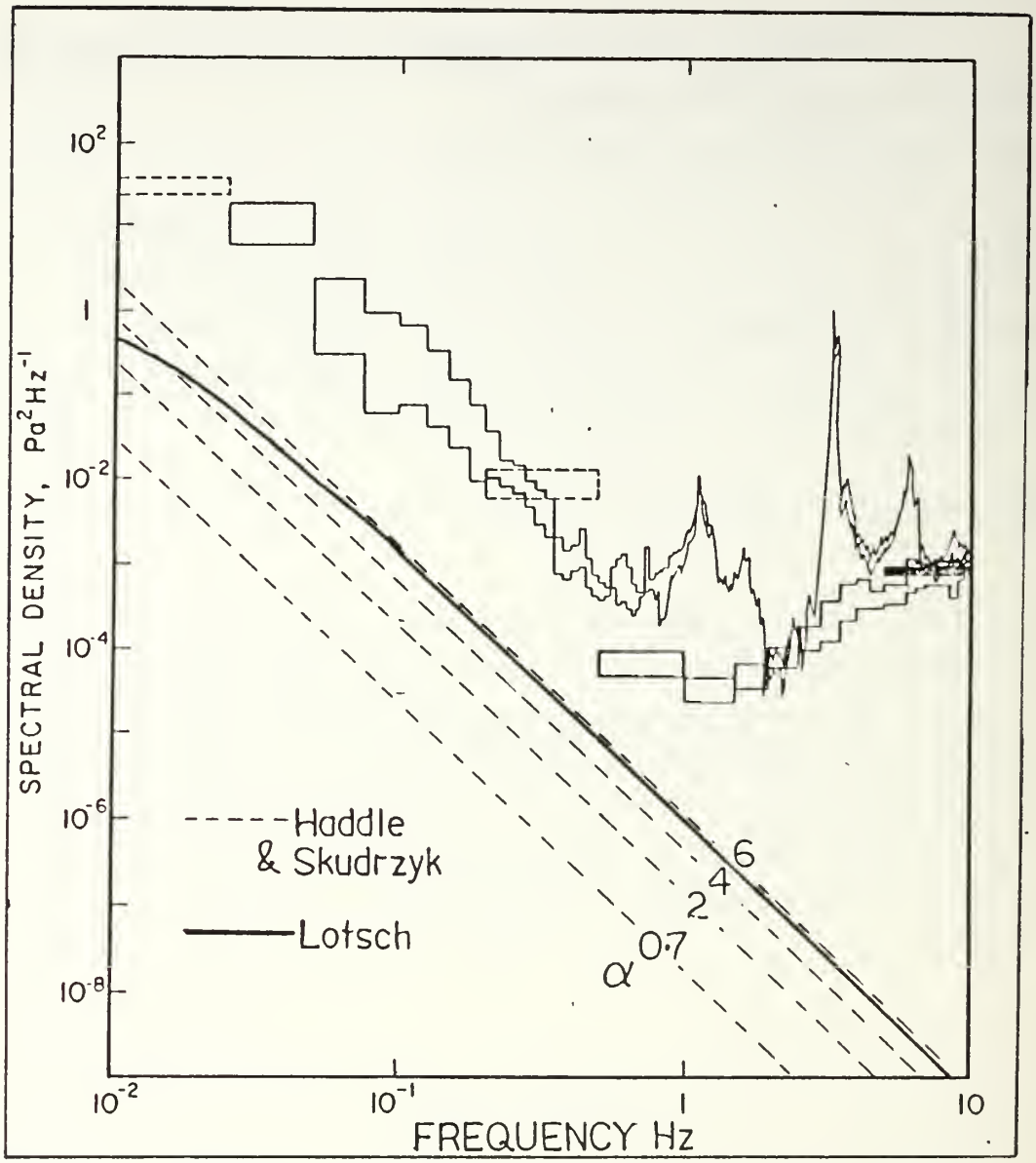

Figure 33. Comparison of the calculated pseudo-sound specta (assuming no roughness) with a measured Arctic noise spectrum.

b. The Effect of Surface Roughness.

The estimates above have assumed the ice sheet to be a smooth flat plate. This is a poor assumption as considerable underside roughness is known to exist (Wadhams, 1988). A commonly assumed value for the roughness scale under ice is 1 m although higher values could be envisaged in some circumstances.

The effect of surface roughness in boundary layer flow is to pierce the laminar sub-layer close to the surface of the boundary. Vortices are shed which pass into the turbulent region, increasing the turbulent motion there and generally shifting noise levels to higher frequencies. These effects begin to be important when the Reynolds number for the flow at the roughness scale exceeds a value of about 5 (Skudrzyk and Haddle, 1960), i.e., when

$$\frac{hU^*}{\nu} \gtrsim 5 \tag{82}$$

where

U^* is the shear velocity, roughly representative of the velocity in the immediate vicinity of the laminar sub-layer, $U^* \simeq 0.04U_0$ (Skudrzyk and Haddle, 1960).

and

h is the length scale for the roughness.

For $h = 1$ m and $U_0 = 0.2$ m s^{-1}

$$\frac{hU^*}{\nu} \simeq 5000 \tag{83}$$

Therefore the rough underside of the ice can be expected to play a major role in the creation of turbulence. The characteristic frequency for pseudo-sound created by roughness is given by

$$f_{0(rough)} = \frac{0.8U_0}{h} \tag{84}$$

rather than the $\frac{0.8U_0}{\delta}$ given by (74) for the flat plate approximation. Thus taking, $U_0 = 0.2$ m s^{-1} and $h = 1$ m, $f_0 \simeq 0.2$ Hz is probably a more reasonable estimate for pseudo-sound under rough ice.

Equations (78), (79) and (81) can now be rewritten for rough boundary conditions. The Skudrzyk and Haddle equations (78) and (79) become

$$P(f) = 1.6\gamma U_0^3 \alpha^2 \delta \quad \text{Pa}^2\text{Hz}^{-1} \qquad f \leq f_{0(rough)} \quad (85)$$

and

$$P(f) = 1.6\gamma U_0^3 \alpha^2 \delta \, (f_{0(rough)}/f)^3 \quad \text{Pa}^2\text{Hz}^{-1} \qquad f > f_{0(rough)} \quad (86)$$

The Lotsch equation (81) becomes

$$P(f) = 6.7\gamma\delta U_0^3 \left(1 + \left(\frac{f\pi h}{5U_0}\right)^2\right)^{-3/2} \quad \text{Pa}^2\text{Hz}^{-1} \quad (87)$$

where

γ is a factor to take into account the increase in the intensity of the turbulent pressure fluctuations due to boundary roughness.

The next problem is to estimate γ. If the noise pressure is broadly proportional to the drag between the boundary and the fluid flowing over it, as suggested by White (1979) γ will be approximately equal to the ratio between the dimensionless drag coefficient in the rough condition and that in the smooth condition. White (1979) gives empirical equations for the dimensionless drag coefficient C_D of a flat plate in both conditions and also presents the relationships graphically (reproduced as Figure 34). $C_{D(smooth)}$ is a function of the Reynolds number for the flow such that

$$C_{D(smooth)} = \frac{0.031}{Re^{1/7}} = 0.031\left(\frac{U_0 L}{\nu}\right)^{-1/7} \tag{88}$$

$C_{D(rough)}$ is independent of Reynolds number in the fully rough condition, depending instead on the parameter L/h (see Figure 34).

$$C_{D(rough)} = (1.89 + 1.62 \log L/h)^{-5/2} \tag{89}$$

L is the horizontal length scale for flow over the plate

h is the roughness scale

An estimate of the increase in pseudo-sound amplitude for a rough surface will therefore be given by the ratio

$$\gamma(U_0, L, h) = \frac{C_{D(rough)}}{C_{D(smooth)}} = \frac{\left(\frac{U_0 L}{\nu}\right)^{1/7}}{0.031(1.89 + 1.62 \log L/h)^{5/2}} \tag{90}$$

Note that this is only valid for fully rough conditions, i.e., the transition $\gamma \rightarrow$ unity for $h \rightarrow 0$ is not described.

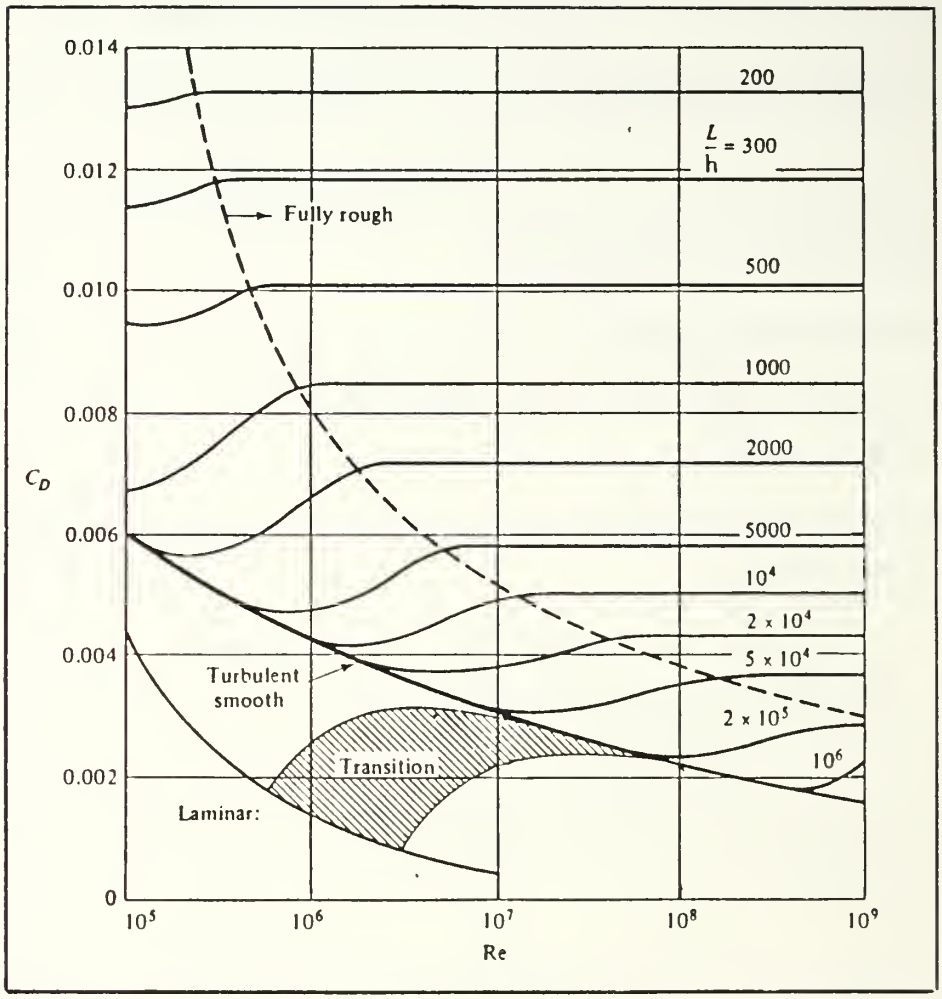

Figure 34. Dimensionless drag coefficients for rough and smooth flat plates (from White, 1979).

Figure 35 shows the calculated pseudo-sound spectra from equations (85) (86) and (87) for a roughness height h = 1m, a boundary layer depth δ = 30 m and a free flow velocity U_0 = 0.2 m s^{-1}. As with the smooth plate approximation, the general shape of the curves fit well with the measured spectrum below 1 Hz. The characteristic frequency f_0 , however, is a little too high suggesting that the effective length scale may in reality lie somewhere between δ and h. Despite this the fit looks promising given the approximate nature of the theory used, and the fact that the input pararameters are crude estimations. This indicates that this mechanism is probably responsible for a large proportion of the noise at these low frequencies. It is worth noting at this point that Makris and Dyer (1986), in a note accompanying their composite ambient noise spectrum, hypothesise that the noise below 1 Hz may be due to non-linear surface wave noise or pseudo-sound in the oceanic boundary layer. No attempt is made to fit a curve exactly to the measured data, as none of the free variables, U_0 , L or h are known for the data set used to produce the composite spectrum.

In conclusion, the indications are that pseudo-sound may well be an important source of noise for hydrophones within the turbulent boundary layer under rough ice, i.e., positioned no more than a few tens of metres below the ice. The frequencies involved are, however, generally below 1 Hz, a region which is not, at present, of general importance.

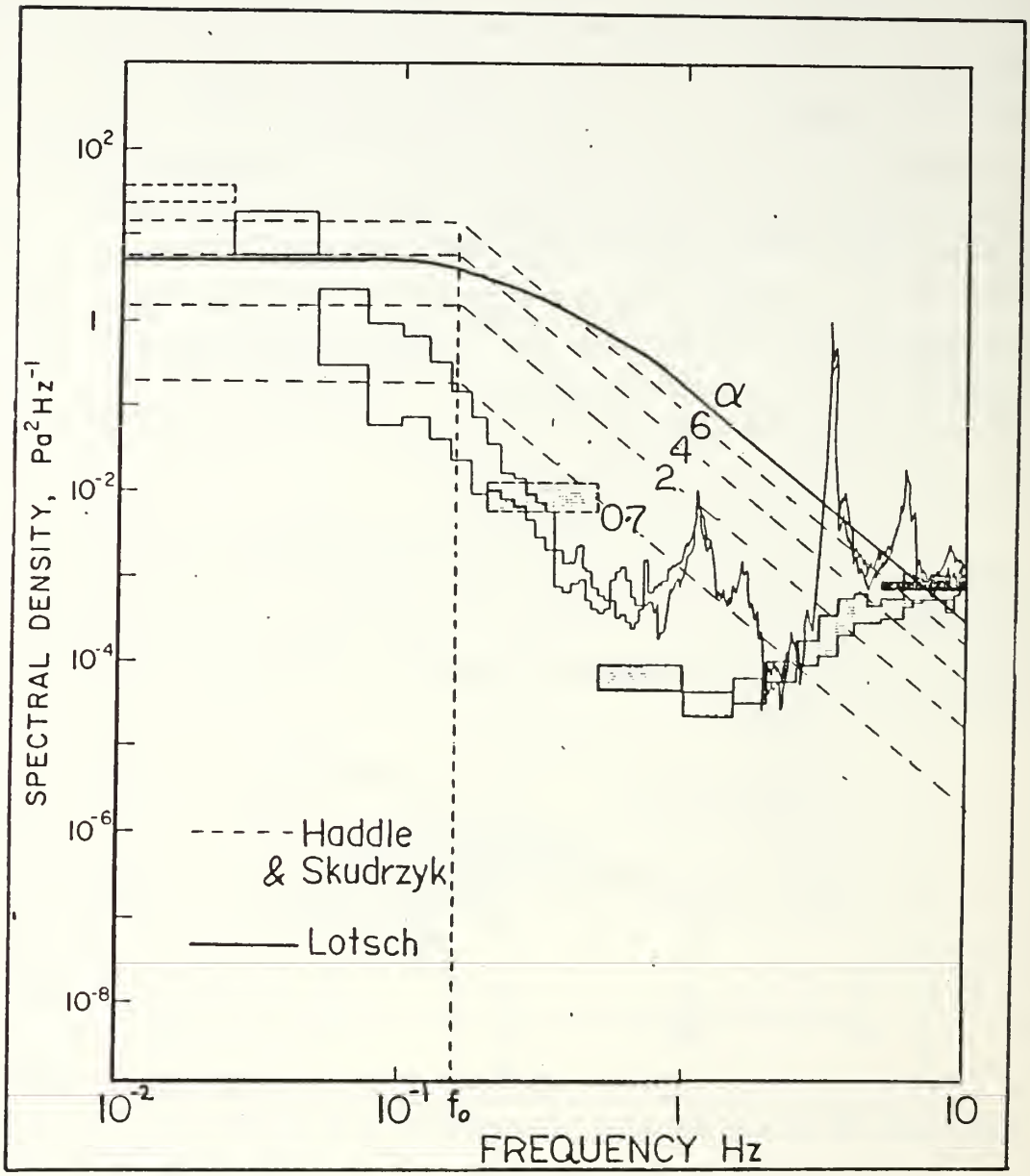

Figure 35. Comparison of the calculated pseudo-sound specta (roughness effects included) with a measured Arctic noise spectrum.

3. **Flow-Induced Noise.**

This is a mechanism by which the effects of turbulent pressure fluctuations are radiated beyond the region of turbulence to the far field. The effect is due to two phenomena. The first occurs within the volume of the turbulent fluid and was described by Lighthill (1954) as being due to quadrapole sources. The second occurs at the interface with a solid boundary and is described as being dipole in nature (Lotsch, 1971). Acoustic power due to the first of these effects is proportional to the eighth power of the Mach number while the power due to the second is proportional to the Mach number squared (Vecchio and Wiley, 1973). In the under-ice environment Mach numbers are very small, typically about 10^{-4}. The dipole sources therefore dominate but the total radiated power is considerably smaller than that due to the turbulent pressure fluctuations themselves. Spherical spreading further reduces sound intensities due to this radiative mechanism. Flow-induced noise is not, therefore, considered to be an important contributor to under-ice noise.

4. **Flow-Excited noise.**

Vecchio and Wiley (1973) identified this mechanism as being another method by which noise can be radiated from a turbulent boundary. The mechanism depends on the presence of turbulent pressure fluctuations along a flexible, elastic boundary. Vibrational modes are excited in the boundary which then radiates sound back into the body of the fluid. Floating ice can certainly be considered as a flexible, elastic boundary; also a preceding section has shown that low frequency pressure fluctuations are created by flow over its rough surface. There exists a possibility, therefore, that this effect might be responsible for noise beyond the turbulent boundary layer immediately under the ice. The physics involved are, however, extremely complex. For this reason no further investigation has been undertaken. Detailed analysis of this process is warranted and may lead to the conclusion that this is a mechanism of some significance.

5. Resonant Cavities.

Water flow past cavities in the under side of an ice sheet is a potential source of noise which must be examined in order to establish its possible importance in the overall creation of ambient noise. Open cavities or orifices in solid boundaries are known to resonate under certain conditions. The onset of resonance depends on the fluid flow velocity past the cavity, the fluid characteristics and the shape and size of the cavity itself. There is water flow past cavities in the under-surface of ice sheets or the submerged surfaces of pressure ridge keels whenever a relative current exists. The object of this investigation is to determine whether this flow is likely to be sufficient to cause noise from such cavities.

a. The Helmholtz Resonator Model.

The Helmholtz resonator is a rigid walled cavity whose resonant properties are known. Theory pertaining particularly to the frequency of resonance as a function of cavity dimensions is used here to model under-ice cavities. Figure 36 shows cross-sections of the classical Helmholtz resonator and an idealized simple cylindrical cavity such as might exist in the under surface of an ice sheet or in a pressure ridge keel.

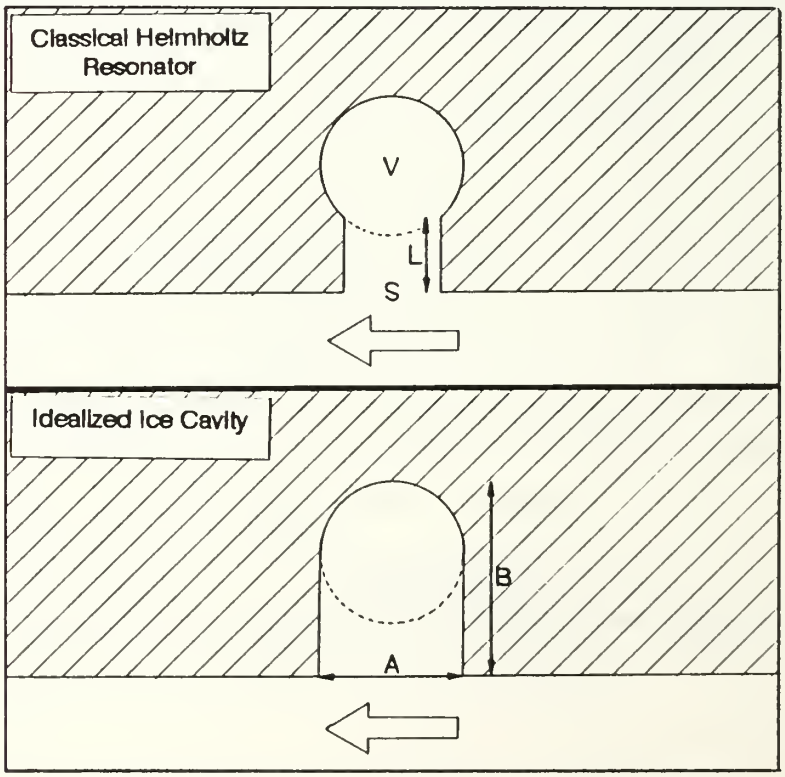

Figure 36. The classical Helmholtz resonantor and a simple cavity.

V is the volume of the inner cavity which provides the *mass* element of the resonator. S: is the area of the circular opening which acts as a simple acoustical source and the fluid in the neck, length L, provides the *stiffness* or *spring* component. From Kinsler et al. (1982) the frequency of resonance is given by

$$\omega_0 = C\left(\frac{S}{L'V}\right)^{1/2} \tag{91}$$

C is the sound speed of the fluid

L' is the effective length of the neck taking radiation -mass loading into account. For practical purposes $L' \simeq L + 0.8A$

A is the diameter of the opening

It is assumed that the acoustic wavelength λ of the sound resulting from resonance is large compared with the length scales L, $S^{1/2}$ and $V^{1/3}$. For the idealized ice cavity

$$L = B - \frac{A}{2} \tag{92}$$

$$S = \pi\left(\frac{A}{2}\right)^2 \tag{93}$$

and

$$V = \frac{4}{3}\pi\left(\frac{A}{2}\right)^3 \tag{94}$$

Therefore

$$\omega_0 = C\left(\frac{15}{10AB - 3A^2}\right)^{1/2}$$

Now taking $C \simeq 1500$ m s^{-1} for sea water

$$\omega_0 \simeq 5810\,(10AB - 3A^2)^{-1/2}$$

and

$$f_0 \simeq 925\,(10AB - 3A^2)^{-1/2} \text{ Hz} \tag{95}$$

The constraint on λ relative to the cavity dimensions dictates that $A \sim B$ for (95) to be valid. Figure 37 shows resonant frequencies for such simple cavities.

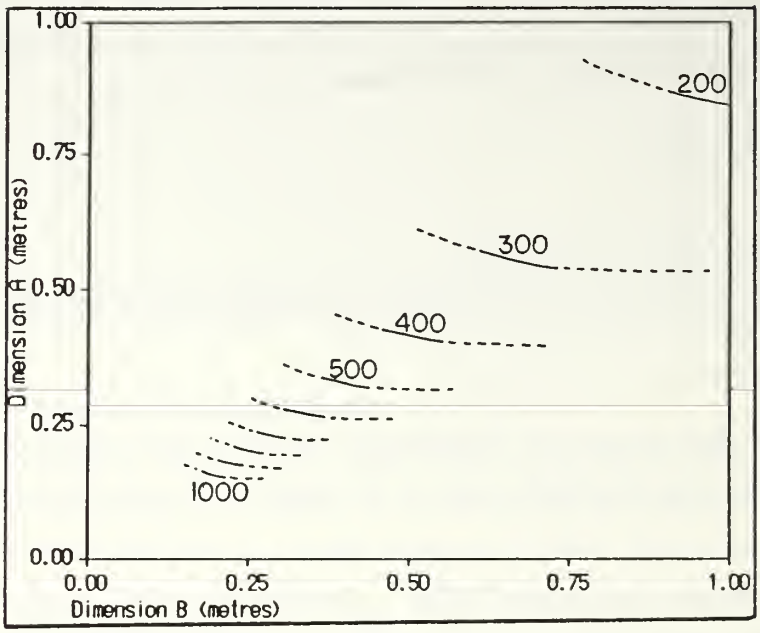

Figure 37. Resonant frequencies (Hz) for simple cavities.

b. Excitation of Resonance.

The next concern is whether the modest flow velocities present under ice are sufficient to excite resonance in the cavities there. From Blake (1984) the relationship between the free-flow velocity across the entrance to a cavity and f_e the frequency of the pressure fluctuations caused by the flow is given by

$$f_e \frac{A}{U_0} = \frac{C_r}{U_0}(n - 1/4) \quad n = 1,2,3,.... \tag{96}$$

U_0 is the free flow fluid velocity

C_r is the hydrodynamic phase velocity across the opening

A is the diameter of the opening

For turbulent boundary layer excitations $\frac{C_r}{U_0} \simeq 0.33$, so

$$f_e \simeq \frac{0.33 U_0}{A}(n - 1/4) \quad n = 1,2,3,.... \tag{97}$$

Figure 38 shows excitation frequencies f_e for cavities up to one metre in diameter. A nominal value of $U_0 = 0.2$ m s^{-1} has been taken to represent a typical maximum relative current velocity under ice.

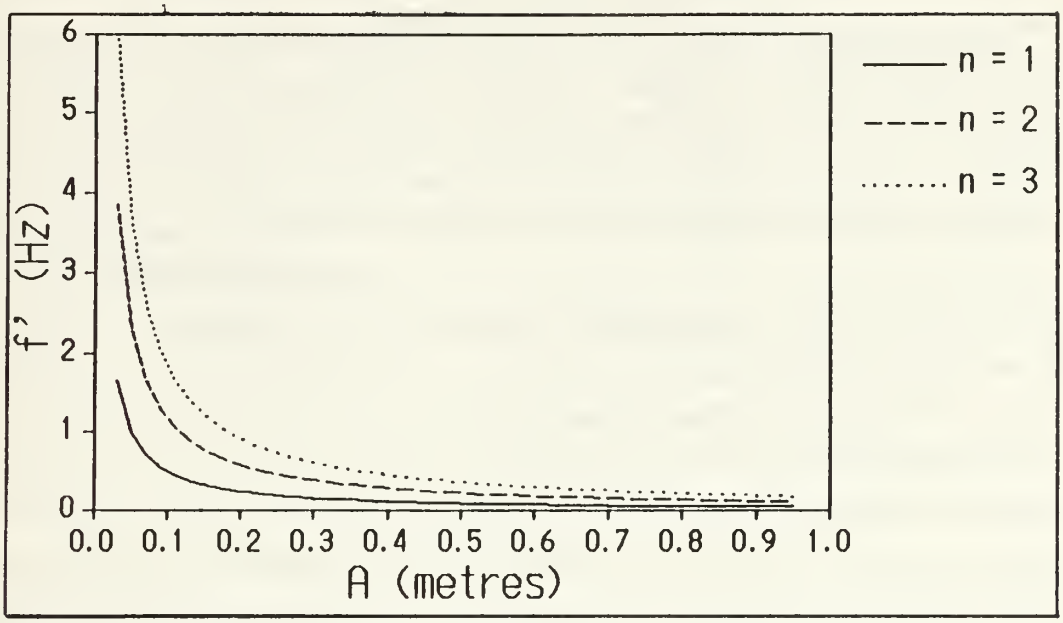

Figure 38. Excitation frequencies for simple cavities (Hz) in a flow velocity of 0.2 m/s.

By comparing Figures 37 and 38 it can be seen that the frequencies at which under-ice cavities could be excited by a typical flow velocity are far lower than their resonant frequencies.

Thus, it is concluded that, within the limits of the approximations made, resonant cavities are unlikely to be important in the generation of ambient noise under ice.

V. SUMMARY AND CONCLUSIONS

The importance of being able to accurately predict ambient noise levels in Arctic waters was discussed in Chapter I. In order to attain that ability research must be undertaken into every aspect of the Arctic ambient noise problem. The reviews of Chapter II and the statements made by Pritchard (1988) illustrate the great number of different subsidiary problems which must be understood and overcome before a reasonable solution can be reached. The large number of possible mechanisms involved in noise generation and their extreme complexity make this a very daunting task. In comparison to the problem of modelling open ocean noise, the Arctic problem is complicated by the different interactive processes between air, ice and sea. In addition, the inaccessability of the Polar regions leads to a dearth of meaningful data. Progress is, however, being made. Wenz (1962) commented on the inadequacy of data from open ocean sites at that time, but was able to describe and catalogue the noise-generating processes to good effect. A similar situation exists now with regard to noise produced in ice-covered waters.

Pritchard (1988) categorized Arctic noise mechanisms into three types by forcing function (as described in Chapter I). This work addresses the mechanisms constituting the third category, i.e., those mechanisms dependent on the shearing of the boundary layer of the ocean under the ice. A scheme is proposed in Chapter III by which this category could be further sub-divided into Flow and Flow/Mechanical mechanisms. The following is a synopsis of the results of investigations into this sub-set of potential noise mechanisms.

A. FLOW/MECHANICAL MECHANISMS.

1. Cracking Noise Due to Wind/Current-Induced Moments.

From statistical work done with observed data, Makris and Dyer (1986) found that ambient noise correlated well with the stress moment acting about an ice sheet's central horizontal plane. In this study, bending moments induced in the ice sheet were investigated by considering the effects of wind and current on an idealized pressure ridge feature. Ridges were envisaged as being in one of two conditions, the young unconsolidated ridge and the more mature consolidated feature. In the case of the first it was found that the moments caused by wind and current are insignificant when compared to the bending moments caused by isostatic loading. The relationship between the bending moments present due to isostatic loading and the critical bending moment re-

quired for cracking in the ice sheet was identified and unstable combinations of ridge height and ice thickness were found. There appeared to be a remote possibility that the wind and current-induced bending moments might act as a precipitative mechanism for cracking actually resulting from isostatic loading. It is felt, however, that this is not a likely explaination for the correlation observed by Makris and Dyer (1986). The study of the consolidated ridge revealed even less likelihood of wind/current-induced cracking through induced bending moments. The assumed rigidity of the system resulted in bending moments that were far below the critical value required for initial cracking.

2. Ice Fragment Bumping

Beyond some observations that ice debris does seem to move about in current-driven motion causing audible sounds, very little appears to have been written on this subject. The concept is attractive in that similar ice-ice interactions are known to cause a great deal of noise at the ice edge. Given sufficient amounts of freely moving fragments and a moderate relative current, a very noisy result could be envisioned. Although the detailed physics of this processes were not investigated, there are indications that the resulting sound would be spread over a wide frequency range, possibly varying from tens of Hz to the low kHz. This is a promising mechanism warranting further investigation. The problem of modelling this effect in practical terms, however, does present many difficulties. The most accute would probably be the determination of the density of free ice fragments in any given region.

B. FLOW MECHANISMS

1. Noise From Turbulence

This is the process by which noise is produced as ice moves in water or when water flows under static ice. It is probably the process envisioned by Lewis and Denner (1988) when they wrote of noise caused by ice "rushing through the water." Investigations of the turbulent pressure fluctuations which could be expected for typical ice roughnesses and flow regimes revealed a predominance of very low frequency activity. When compared to a measured Arctic spectrum, the predicted turbulent pressure or pseudo-sound spectra have the correct characteristics to explain low frequency noise. Thus it is suspected that pseudo-sound in the boundary layer is significant at frequencies below 1 Hz but only for receivers actually within the region of turbulence.

Two mechanisms, Flow-Induced and Flow-Excited noise, by which the effects of turbulent pressure fluctuations might be radiated were mentioned briefly. The first appears to be too inefficient to radiate significant sound energy. The second may, how-

ever, be of some importance. Both phenomena need further, more detailed, consideration.

2. Resonant Cavities

The idea that cavities in the under surface of the ice might resonate due to water flow comes from a consideration of similar features in air. A comparison with the classical Helmholtz resonator concept revealed the likely frequencies of resonance for various cavity dimensions. By establishing the frequencies that typical flow velocities might excite, however, it was found that such flows are almost certainly too slow to cause resonance. Thus this mechanism is considered to be an unlikely candidate for noise production.

APPENDIX BEAMS ON ELASTIC FOUNDATIONS.

This appendix describes the theoretical behaviour of infinite and semi-infinite beams on elastic foundations as given by Hetenyi (1946). This theory is used to model floating ice because the ice is flexible to a degree and since buoyancy and gravity make the sea act like an elastic foundation.

A. INFINITE BEAMS.

The spatial distribution of displacement, $y(x)$, slope $\theta(x)$, bending moment $M(x)$ and shear force $Q(x)$ for an infinite beam, on an elastic foundation, subjected to a point loading P and moment M (see Figure 39) are given by:-

$$y(x) = \frac{P\lambda}{2k} A_{\lambda x} + \frac{M\lambda^2}{k} B\lambda x \qquad (A1)$$

$$\theta(x) = -\frac{P\lambda^2}{k} B_{\lambda x} + \frac{M\lambda^3}{k} C_{\lambda x} \qquad (A2)$$

$$M(x) = \frac{P}{4\lambda} C_{\lambda x} + \frac{M}{2} D_{\lambda x} \qquad (A3)$$

$$Q(x) = -\frac{P}{2} D_{\lambda x} - \frac{M\lambda}{2} A_{\lambda x} \qquad (A4)$$

where

k is the foundation modulus $= (\rho_w - \rho_i)g$ for floating ice (A5)

$1/\lambda$ is the characteristic length of the system $= \left(\frac{4EI}{k}\right)^{1/4}$ m^{-1} (A6)

E is the Youngs modulus for the material of the beam per unit width

I is the moment of inertia for the beam $= \frac{t^3}{12}$ (A7)

t is the thickness of the beam.

$$A_{\lambda x} = e^{-\lambda x}(\cos \lambda x + \sin \lambda x) \tag{A8}$$

$$B_{\lambda x} = e^{-\lambda x} \sin \lambda x \tag{A9}$$

$$C_{\lambda x} = e^{-\lambda x}(\cos \lambda x - \sin \lambda x) \tag{A10}$$

$$D_{\lambda x} = e^{-\lambda x} \cos \lambda x \tag{A11}$$

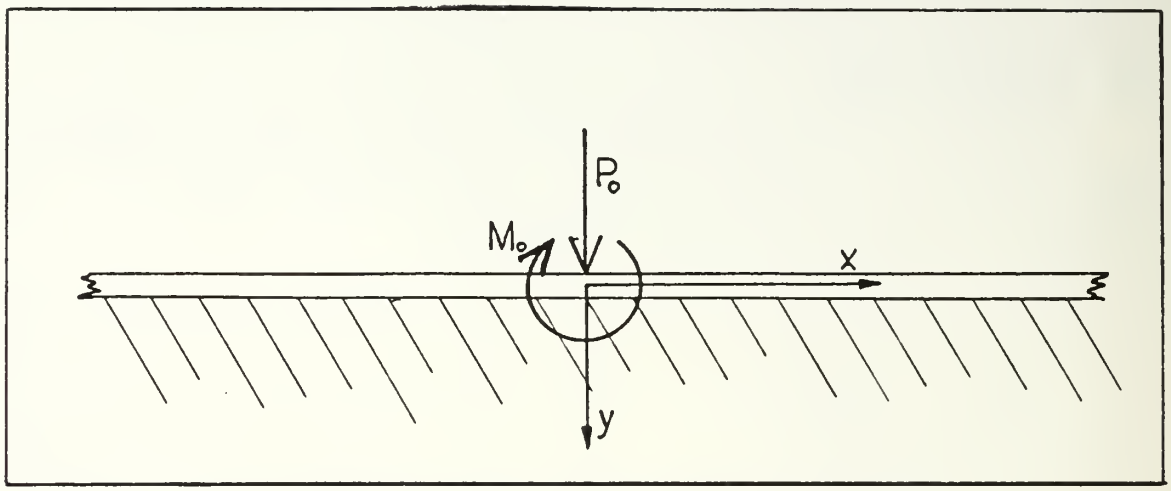

Figure 39. The infinite beam with a point load and bending moment.

B. INFINITE BEAMS WITH TRIANGULARLY DISTRIBUTED LOADINGS.

For a triangularly distributed loading (see Figure 40)

$$y(x) = \frac{q_0}{4k\lambda\ell}(C_{\lambda|\ell-x|} - C_{\lambda x} - 2\lambda\ell D_{\lambda x} + 4\lambda(\ell - x)) \qquad 0 \le x < \ell \tag{A12}$$

$$y(x) = \frac{q_0}{4k\lambda\ell}(C_{\lambda|\ell-x|} - C_{\lambda x} - 2\lambda\ell D_{\lambda x}) \qquad x \ge \ell \tag{A13}$$

$$M(x) = -\frac{q_0}{8\lambda^3\ell}(A_{\lambda|\ell-x|} - A_{\lambda x} - 2\lambda\ell B_{\lambda x}) \qquad x \ge 0 \tag{A14}$$

$$Q(x) = -\frac{q_0}{4\lambda^2\ell}(B_{\lambda|\ell-x|} + B_{\lambda x} - \lambda\ell C_{\lambda x}) \qquad x \ge 0 \tag{A15}$$

where

q_0 is the load at $x = 0$

ℓ is the base length of triangular loading

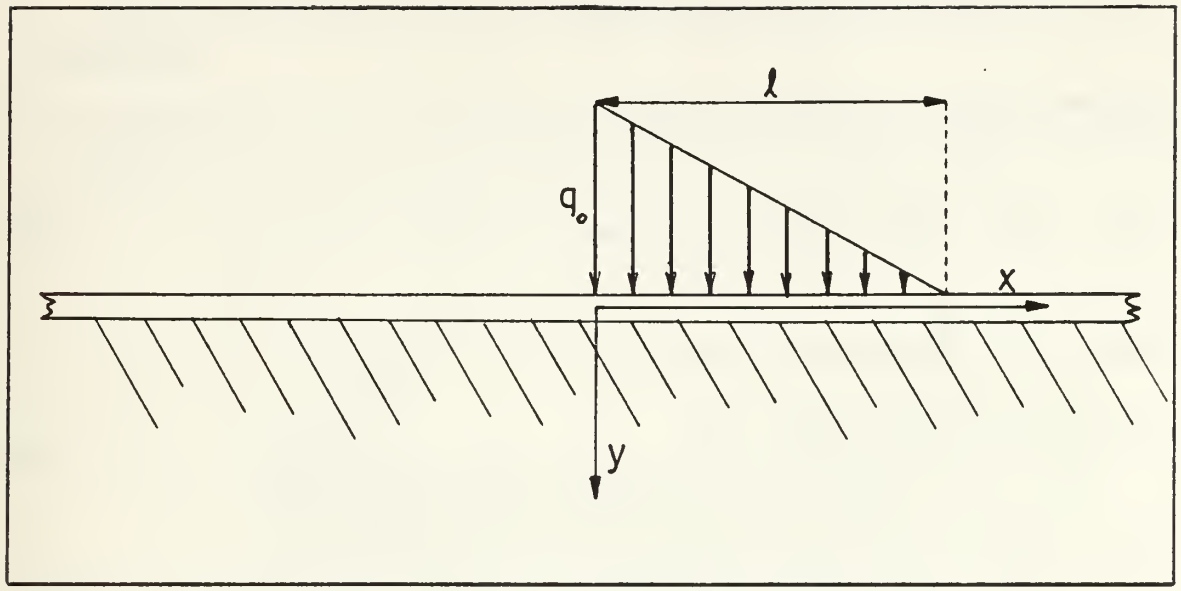

Figure 40. Infinite beam with triangularly distributed loading.

C. SEMI-INFINITE BEAMS WITH TRIANGULARLY DISTRIBUTED LOADINGS.

If the infinite beam equations, (A1) to (A4), are to be used to describe a semi-infinite beam with a triangular loading, end conditioning forces must be applied in order to create the effect of a free end. Thus, if a free end is to be created at $x = 0$, a force P' and moment M' must be applied to exactly cancel Q_0 and M_0. The result will then be $M(0) = 0$ and $Q(0) = 0$, the conditions for a free end. From (A14) and (A15) at $x = 0$

$$M_0 = -\frac{q_0}{8\lambda^3\ell}(A_{\lambda\ell} - 1) \qquad (A16)$$

$$Q_0 = -\frac{q_0}{4\lambda^2\ell}(B_{\lambda\ell} - \lambda\ell) \qquad (A17)$$

Substituting (A16) and (A17) into (A3) and (A4), with $x = 0$

$$M(0) = \frac{P'}{4\lambda} + \frac{M'}{2} + \frac{q_0}{8\lambda^2 \ell}(A_{\lambda\ell} - 1) = 0 \qquad (A18)$$

$$Q(0) = \frac{-P'}{2} - \frac{M'\lambda}{2} - \frac{q_0}{4\lambda^2 \ell}(B_{\lambda\ell} - \lambda\ell) = 0 \qquad (A19)$$

Solving (A18) and (A19) for P' and M'

$$P' = \frac{q_0}{2\lambda^2 \ell}(-A_{\lambda\ell} + 1 - 2B_{\lambda\ell} + 2\lambda\ell) \qquad (A20)$$

$$M' = -\frac{q_0}{2\lambda^3 \ell}(-A_{\lambda\ell} + 1 - B_{\lambda\ell} + \lambda\ell) \qquad (A21)$$

The distribution of displacement on the semi-infinite beam with a triangular loading can now be found by superimposing the effect of the load from (A12), together with the effects of P' and M' at $x = 0$ as described by (A1).

$$y(x) = \frac{q_0}{4k\lambda\ell}(C_{\lambda|\ell-x|} - C_{\lambda x} - 2\lambda\ell D_{\lambda x} + 4\lambda(\ell - x)) + \frac{P'\lambda}{2k} A_{\lambda x} + \frac{M'}{k} B_{\lambda x} \quad 0 \le x < \ell \; (A22)$$

$$y(x) = \frac{q_0}{4k\lambda\ell}(C_{\lambda|\ell-x|} - C_{\lambda x} - 2\lambda\ell D_{\lambda x}) + \frac{P'\lambda}{2k} A_{\lambda x} + \frac{M'}{k} B_{\lambda x} \qquad x \ge \ell \; (A23)$$

Substituting for P' and M' and simplifying

$$y(x) = \frac{q_0}{4k\lambda\ell}(C_{\lambda|\ell-x|} + 4\lambda(\ell - x) + B_{\lambda x}A_{\lambda\ell} - D_{\lambda x}(A_{\lambda\ell} + 2B_{\lambda\ell})) \qquad 0 \le x < \ell \; (A24)$$

$$y(x) = \frac{q_0}{4k\lambda\ell}(C_{\lambda|\ell-x|} + B_{\lambda x}A_{\lambda\ell} - D_{\lambda x}(A_{\lambda\ell} + 2B_{\lambda\ell})) \qquad x \ge \ell \; (A25)$$

And since $M(x) = -EI\dfrac{d^2y}{dx^2}$ (from Hetenyi)

$$M(x) = -\frac{q_0}{8\lambda^3 \ell}(A_{\lambda|\ell-x|} - D_{\lambda x}A_{\lambda\ell} - B_{\lambda x}(A_{\lambda\ell} + 2B_{\lambda\ell})) \qquad x \ge 0 \; (A26)$$

D. SEMI-INFINITE BEAMS WITH POINT LOADINGS AND BENDING MOMENTS.

Developments similar to those describing the behaviour of a semi-infinite beam with a triangularly distributed loading are used in the case of a point loading and bending moment at the free end (see Figure 41).

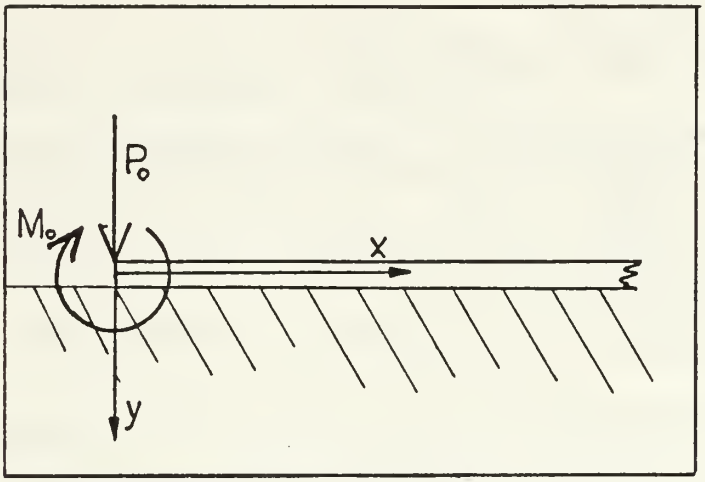

Figure 41. Semi-infinite beam with a point loading and bending moment.

Equations for the displacement, slope, bending moment and shear force distibutions are given below.

$$y(x) = \frac{2P\lambda}{k} D_{\lambda x} - \frac{2M\lambda^2}{k} C_{\lambda x} \qquad (A27)$$

$$\theta(x) = -\frac{2Q\lambda^2}{k} A_{\lambda x} + \frac{4M\lambda^3}{k} D_{\lambda x} \qquad (A28)$$

$$M(x) = -\frac{P}{\lambda} B_{\lambda x} + M A_{\lambda x} \qquad (A29)$$

$$Q(x) = -PC_{\lambda x} - 2M\lambda B_{\lambda x} \qquad (A30)$$

REFERENCES

Blake, K., 1986. Aero-Hydrodynamics for ships vol. 1. David Taylor Naval Ship Research and Development Center.

Buck, B.M. and Wilson, J.H., 1986. Nearfield noise measurements from an Arctic pressure ridge. Journal of the Acoustical Society of America, 80 (1), 256-264.

Diachok, O.I. and Winokur, R.S., 1974. Spatial variability of underwater ambient noise at the ice-water boundary. Journal of the Acoustical Society of America, 55 (4), 750-753.

Ganton, J.H. and Milne, A.R., 1965. Temperature- and wind-dependent ambient noise under midwinter pack ice. Journal of the Acoustic Society of Amaerica, 38(2), 406-411.

Hannah, J. and Hillier, M.J., 1970. Mechanical engineering science. Pitman, London, 443 p.

Hetenyi, M., 1946. Beams on elastic foundation. University of Michigan Press, 255 p.

Kinsler, L.E., Frey, A.R., Coppens, A.B. and Sanders, J.V., 1982. Fundamentals of acoustics. John Wiley and Sons, New York.

Lewis, J.K. and Denner, W.W., 1988. Arctic ambient noise in the Beaufort Sea: relationships to sea ice kinematics. Journal of the Acoustical Society of America, 83 (2), 549-565.

Lighthill, M.J., 1954. On sound generated aerodynamically II. Turbulence as a source of sound. Proceedings of the Royal Society, A 222, 1-31.

Lotsch, H.K.V., 1971. Pseudo-sound in a plane, turbulent boundary-layer flow. Bull. American Physical Society, 16 (II), 1323.

Makris, N.C. and Dyer, I.D., 1986. Environmental correlates of pack ice noise. Journal of the Acoustical Society of America, 79 (5), 1434-1440.

Mellor, M., 1986. Mechanical behavior of sea ice. Chapter 2 in, The geophysics of sea ice, ed. Untersteiner, N. Plenum Press, New York, 165-281.

Milne, A.R., 1972. Thermal tension cracking in sea ice: a source of underice noise. Journal of Geophysics Research, 77(12), 2177-2192.

Oard, V.T., June 1987. Characteristic spectral signatures of Arctic noise-generating mechanisms. Masters Thesis, Naval Postgraduate School, Monterey, CA.

Paquette, R.G. and Bourke, R.H., 1988. Deflection of sea ice due to ridging. (unpublished).

Payne, F.A., 1964. Effect of ice cover on shallow-water ambient sea noise. Journal of the Acoustical Society of America, 36 (10), 1943-1947.

Pritchard, R.S., 1988. Modelling Arctic underice ambient noise. (unpublished).

Pritchard, R.S., 1984. Arctic Ocean background noise caused by ridging of ice. Journal of the Acoustical Society of America, 75 (2), 419-427.

Ross, D., 1987. Mechanics of underwater noise. Peninsula Publishing, Los Altos, CA, 375 p.

Shepard, G.W., 1979. Arctic ocean ambient noise. Ocean Engineer's Thesis, Massachusetts Institute of Technology, Cambridge, MA.

Skudrzyk, E.J. and Haddle, G.P., 1960. Noise production in a turbulent boundary layer by smooth and rough surfaces. Journal of the Acoustical Society of America, 32 (1), 19-34

Urick, R.J., 1983. Principles of underwater sound. McGraw-Hill, New York, 423p.

Vecchio, E.A. and Wiley, C.A., 1973. Noise radiated from a turbulent boundary layer. Journal of the Acoustical Society of America, 53 (1), 596-601.

Waddell, S.R. and Farmer, D.M., 1988. Ice breakup: observations of the acoustic signal. Journal of Geophysical Research, 93 (C3), 2333-2342.

Wadhams, P., 1988. The underside of Arctic sea ice imaged by sidescan sonar. Nature, 333 (12), 161-164.

Wenz, G.M., 1972. Review of underwater acoustic research: noise. Journal of the Acoustical Society of America, 51 (3,part 2), 1010-1024.

Wenz, G.M., 1962. Acoustic ambient noise in the ocean: spectra and sources. Journal of the Acoustical Society of America, 34 (12), 1936-1956.

White, F.M., 1986. Fluid mechanics. McGraw-Hill, New York, 732p.

Wright, B.D., Hnatiuk, J. and Kovacs, A., 1978. Sea ice pressure ridges in the Beaufort Sea. United States Army Corps of Engineers Cold Regions Research and Engineering Laboratory.

Young, O.R., 1986. The age of the Arctic. Oceanus, 29 (1), Woods Hole Oceanographic Institution, Woods Hole, MA, 9-17.

Zubov, N.N., 1943. Arctic ice. Moscow, USSR, tr. by U.S. Naval Oceanographic Office and the American Meteorological Society.

INITIAL DISTRIBUTION LIST

		No. Copies
1.	Defense Technical Information Center Cameron Station Alexandria, VA 22304-6145	2
2.	Library, Code 0142 Naval Postgraduate School Monterey, CA 93943-5002	2
3.	Chairman (Code 63Rd) Department of Meteorology Naval Postgraduate School Monterey, CA 93943-5000	1
4.	Chairman (Code 68Co) Department of Oceanography Naval Postgraduate School Monterey, CA 93943-5000	1
5.	Professor Jeffrey A. Nystuen (Code 68Ny) Department of Oceanography Naval Postgraduate School Monterey, CA 93943-5000	2
6.	Professor Robert H. Bourke (Code 68Bf) Department of Oceanography Naval Postgraduate School Monterey, CA 93943-5000	2
7.	Dr. Robert S. Pritchard Icecasting, Inc. 11042 Sand Point Way N.E. Seattle, WA 98125-5846	4
8.	Director of Naval Oceanography and Meteorology Lacon House Theobalds Road London WC1X 8RY United Kingdom	2
9.	Officer-in-Charge Oceanographic Centre CINCFLEET Northwood Middlesex United Kingdom	2

10. Officer-in-Charge 1
RNSOMO
RNAS Culdrose
Helston
Cornwall
United Kingdom

11. Dr D. Williams 1
Staff of CBNSW
British Embassy
3100 Massachusetts Avenue NW
Washington, DC 20008

12. Lt. Stephen J. Hipsey, RN 1
Oceanographic Centre
CINCFLEET
Northwood
Middlesex
United Kingdom

13. Library 1
Institute of Oceanographic Sciences
Brook Road
Wormley, Godalming
Surrey GU8 5UB
United Kingdom

14. Director Naval Oceanography Division 1
Naval Observatory
34th and Massachusetts Avenue NW
Washington, DC 20390

15. Commander 1
Naval Oceanography Command
NSTL Station
Bay St. Louis, MS 39522

16. Commanding Officer 1
Naval Oceanographic Office
NSTL Station
Bay St. Louis, MS 39522

17. Commanding Officer 1
Fleet Numerical Oceanography Center
Monterey, CA 93943

18. Commanding Officer 1
Naval Environmental Prediction Research Facility
Monterey, CA 93943

19. Chairman, Oceanography Department
U. S. Naval Academy
Annapolis, MD 21402 — 1

20. Chief of Naval Research
800 North Quincy Street
Arlington, VA 22217 — 1

21. Office of Naval Research (Code 420)
Naval Ocean Research and Development Activity
800 North Quincy Street
Arlington, VA 22217 — 1

22. Commanding Officer
Naval Polar Oceanography Center
Suitland
Washington, DC 20373 — 1

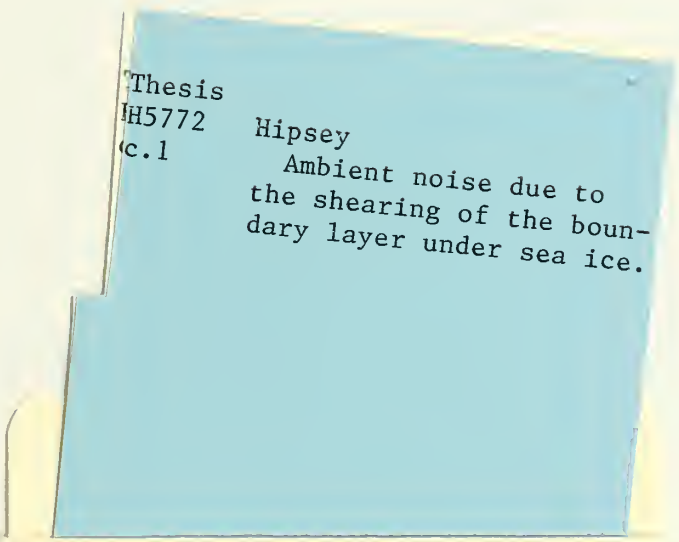

Thesis
H5772
c.1
Hipsey
Ambient noise due to
the shearing of the boun-
dary layer under sea ice.